RESEARCH INVESTIGATION OF LASER LINE PROFILES (PICOSECOND LASER PULSES)

William H. Glenn

United Aircraft Research Laboratories

Prepared for:

Office of Naval Research
Advanced Research Projects Agency

1 March 1974

Unclassified

SECURITY CLASSIFICATION OF THIS PAGE (When Data Entered)

REPORT DOCUMENTATION PAGE		READ INSTRUCTIONS BEFORE COMPLETING FORM
1. REPORT NUMBER N-920479-44	2. GOVT ACCESSION NO.	3. RECIPIENT'S CATALOG NUMBER AD 775576
4. TITLE (and Subtitle) LASER LINE PROFILES (Picosecond Laser Pulses)		5. TYPE OF REPORT & PERIOD COVERED Final 8/1/66 - 2/28/74 6. PERFORMING ORG. REPORT NUMBER
7. AUTHOR(s) W. H. Glenn		8. CONTRACT OR GRANT NUMBER(s) N00014-66-C-0344
9. PERFORMING ORGANIZATION NAME AND ADDRESS United Aircraft Research Laboratory 400 Main Street East Hartford, Conn. 06108		PROGRAM ELEMENT, PROJECT, TASK AREA & WORK UNIT NUMBERS ARPA Order #1806 AMEND #9
11. CONTROLLING OFFICE NAME AND ADDRESS Office of Naval Research Department of the Navy Arlington, VA 22217		12. REPORT DATE 3/1/74 13. NUMBER OF PAGES 60
14. MONITORING AGENCY NAME & ADDRESS (if different from Controlling Office) Director, Physics Program Office of Naval Research		15. SECURITY CLASS. (of this report) Unclassified 15a. DECLASSIFICATION DOWNGRADING SCHEDULE

16. DISTRIBUTION STATEMENT (of this Report)

Unlimited

17. DISTRIBUTION STATEMENT (of the abstract entered in Block 20, if different from Report)

18. SUPPLEMENTARY NOTES

19. KEY WORDS (Continue on reverse side if necessary and identify by block number)

Picosecond Optical Pulses
Imaging Optical Radar

20. ABSTRACT (Continue on reverse side if necessary and identify by block number)

This report discusses the application of picosecond optical pulses to high resolution imaging optical radar. A novel type of signal processing is described. An extensive bibliography of previous work on this contract is included.

DD FORM 1 JAN 73 1473 EDITION OF 1 NOV 65 IS OBSOLETE

Unclassified

SECURITY CLASSIFICATION OF THIS PAGE (When Data Entered)

60

UNITED AIRCRAFT CORPORATION
RESEARCH LABORATORIES

Report Number: N-920479-44
Final Technical Report for the Period
1 August 1966 to 28 February 1974

PICOSECOND LASER PULSES

ARPA Order No.	1806 AMEND #9/11-15-72
Program Code:	3E90
Contractor:	United Aircraft Research Laboratories
Eifective Date of Contract:	1 August 1966
Contract Expiration Date:	1 March 1974
Amount of Contract:	$581,628
Contract Number:	N00014-66-C-0-344
Principal Investigator:	Dr. William H. Glenn (203) 565-5411
Scientific Officer:	Dr. Robert E. Behringer
Short Title:	Picosecond Laser Pulses
Reported by:	W. H. Glenn

Sponsored By
Advanced Research Projects Agency
ARPA Order No. 1806

United Aircraft Research Laboratories
Final Report N-920479-44
For the Period 1 August 1966 to 28 February 1974

TABLE OF CONTENTS

N920479-44

TECHNICAL REPORT SUMMARY

This report is the last in a series of reports under Contract N00014-66-C0344. This contract has been active for nearly eight years, from 1 August 1966 to 28 February 1974. During this period of time the emphasis has changed a number of times. Topics which have been covered include laser line profiles, coherent propagation effects (pi pulse propagation and adiabatic rapid passage), picosecond pulse phenomena, dynamic spectroscopy, nonlinear optical effects, transient stimulated scattering effects (Rayleigh and Raman) organic dye lasers, stable Nd:Yag laser and most recently, coherent imaging optical radar techniques using picosecond laser pulses. It is impossible in a reasonable amount of space to review all of this work in detail. An indication of the scope of the effort is provided by the list of 54 publications and major presentations that have resulted from this work (Appendix I). This report will discuss in detail only the most recent portion of the work involving coherent imaging optical radars. The reader is referred to previous reports in this series for a detailed discussion of earlier work on this contract. During the course of this contract, the contributors have been, in alphabetical order, M. J. Brienza, A. R. Clobes, A. J. DeMaria, C. M. Ferrar, W. H. Glenn, G. L. Lamb, Jr., M. E. Mack, E. B. Treacy and D. A. Stetser.

The most recent portion of the work in this contract has been an investigation of the application of picosecond optical pulses to imaging optical radars. Microwave synthetic aperture radars (SAR) achieve spatial resolution that is much better than that determined by the diffraction limit of the transmitted beam. This is accomplished by range-doppler processing of the received signal; the technique is useful whenever there is relative motion between the transmitter and the target. An SAR uses a wide bandwidth transmitted signal to achieve downrange resolution and doppler processing to achieve crossrange resolution. This technique can be applied to an optical radar. The higher carrier frequency allows much better doppler resolution and the wider bandwidth available allows much better time resolution. Lasers are available to generate sub-picosecond pulses; a one picosecond pulse corresponds to a range resolution of .015 cm so that the use of such pulses in a range-doppler system is potentially capable of producing images of photographic quality at a range that is limited only by the available laser power.

Section 1 of this report reviews briefly the range-doppler processing scheme and discusses an experiment in which a mode-locked Nd-Yag laser was used to obtain a range doppler image of a small laboratory target with 1-2 cm resolution.

To apply microwave SAR techniques directly to an optical radar would require an optical detector and subsequent signal processing electronics with a bandwidth comparable to that of the received signal. This bandwidth could be as high as 10^{12} Hz and is far beyond present capabilities. It is possible, however, by optical preprocessing of the received signal prior to detection, to reduce the required bandwidth by orders of magnitude. This is possible because the information bandwidth of the signal is much less than the bandwidth required for range resolution.

Section 2 of this report describes such a system. It basically involves an optical Fourier analysis of the received signal prior to detection. It is capable of arbitrarily high time resolution (limited only by the laser) and does not require fast detectors. It can also achieve optimum (quantum noise limited) detection efficiency. An experiment demonstrating the principle of this system is discussed. This experiment demonstrated the ability of the system to resolve sub-nanosecond signals with slow detectors and to present a time expanded version of the signal for direct observation. The major importance of this result is that it is possible, with slow detectors and electronics, to process an extremely fast optical signal in an efficient way. The resolution of an optical SAR should thus be limited only by the bandwidth and coherence of the laser and not by the response time of the receiver.

SECTION 1

IMAGING OPTICAL RADARS

This contract has been concerned with the application of extremely short duration optical pulses to imaging radars. The problem that has been considered is that of imaging a target whose size and distance is such that it cannot be resolved by conventional optical imaging. If there is relative motion between the target and the radar transmitter, range-doppler processing of the received signal may be used to generate a two dimensional image of the target. The situation is illustrated schematically in Figure 1a. The target is taken to be a collection of scattering centers that are rotating as a rigid body about an axis of rotation. If the received energy is analyzed in time and frequency, a range-doppler image of the target may be constructed as shown in Figure 1b. The contours of constant range are lines perpendicular to the line-of-sight between the transmitter and the target, while the contours of constant doppler shift are parallel to the line of sight. Together, they impose a coordinate system on the target which is used to generate the image. In this simplified case, the image looks exactly like the target. For more complicated, three dimensional targets, the situation is more complicated, but the range-doppler image still gives the projection of the target on the down-range and cross-range directions.

The resolution in the down-range direction is determined by the time resolution. of the radar; i.e., by the reciprocal of the bandwidth of the transmitted waveform. If the bandwidth is B, then

$$\Delta x = \frac{c}{2B}$$

The resolution in the cross range direction depends on how well the doppler frequencies can be resolved. The doppler shift for a scatterer located at position y is

$$\omega_d = \frac{2\omega v}{c} = \frac{2\omega\Omega y}{c}$$

where Ω is the rotation rate and ω is the optical frequency. If the target is observed for a time τ, then the minimum resolvable doppler shift is $\delta\omega \approx 2\pi/t$. We have then

$$\frac{2\omega\Omega}{c}\,\Delta y > \frac{2\pi}{t}$$

$$\Delta y > \frac{2\pi c}{2\omega\Omega t} = \frac{\lambda}{2\Omega\theta}$$

where $\theta = \Omega t$ is the angle through which the target has turned in the time T. Both Δx and Δy are independent of the range of the target in contrast to the resolution of a conventional imaging system where the minimum resolvable element size increases linearly with range. The magnitude of the doppler shift is

$$\omega_d = 4\pi \frac{y}{\lambda} \Omega$$

For a target size of 1 meter

$$\omega_d = 4\pi \times 10^6 \Omega \text{ at } \lambda = 1.06\,\mu$$
$$= 4\pi \times 10^5 \Omega \text{ at } \lambda = 10.6\,\mu .$$

Laser bandwidths of $\sim$ 1 GH_z are presently available in CO_2 lasers at 10.6μ, and it is expected that much larger bandwidths will be available in the future. Neodymium-YAG lasers have bandwidths that could give time resolutions of $\sim$ 50 psec. A time resolution of 100 psec corresponds to a range resolution of 1.5 cm, and 1 psec to 0.015 cm. Optical radars are thus potentially capable of extremely high spatial resolution. In order to take advantage of this very high resolution, means for processing extremely fast optical transients must be developed. Most of the effort on this contract has been concerned with this problem. Although the bandwidth of the transmitted signal is necessarily very large if high resolution is desired, the actual information rate is not. The information desired from the received signal is an image of the target. If we assume that we want an image with 100 resolvable elements, each with a 10 bit gray scale and that we obtain the image in 1 millisecond, then the actual information rate is $\sim 10^6$ bits/sec. This is far less than the bandwidth of the transmitted waveform which could be 10^{12} Hz or higher. This observation leads to the conclusion that with proper signal processing, the desired image could be obtained with a relatively slow detection system.

A variety of waveforms could be used to obtain an image of the target. As mentioned above, the down range resolution is determined by the reciprocal of the bandwidth B of the signal and the cross range resolution by the total duration τ of the signal. The "average resolution" can be taken as

$$(\Delta x \Delta y)^{\frac{1}{2}} \sim (BT)^{-\frac{1}{2}}$$

so that all signals with the same time-bandwidth product are equivalent as far as resolution. One possibility is to use a periodic train of short pulses that can be obtained conveniently from a mode-locked laser. This situation is illustrated in Figure 2a. The time between the pulses, if derived from a mode-locked laser, would typically be a few nanoseconds. The received signal will consist of a quasi-periodic train of longer duration pulses as shown in Figure 2b. Each of these pulses is a narrow band signal in times of the optical center frequency, and can be described in terms of an envelope $f(t)$ and an instantaneous phase $\Phi(t)$. Adjacent received pulses

are nearly identical but there is a slow variation of f and ϕ that occurs over a time corresponding to the reciprocal of the doppler spread. The corresponding frequency domain description of the transmitted and received signals is shown in Figure 3.

One way of processing this signal is to range gate it and measure the amplitude and phase within each range element. Frequency analysis of the amplitude and phase within each range element gives the doppler spectrum within that range element. Measurements on each range element may then be used to construct the range-doppler image of the target. The signal could be processed by the scheme shown in Figure 4a. The signal is heterodyned against a local oscillator, detected, and range gated. If the local oscillator is at the same center frequency as the signal, a quadrature channel with the local oscillator shifted by $\lambda/4$ is also needed. If there is a frequency offset, this is not necessary. For a stationary target, the output of each range element will vary at the offset frequency and will be proportional to the signal received in that range element. If the target is rotating, the doppler spectrum from each range element will be superimposed on the signal. In this system, the detectors and the range gating electronics must be sufficiently fast to accommodate the desired time resolution of the received signal.

An alternate scheme is shown in Figure 4b. Here the signal is heterodyned against a mode-locked local oscillator which may be derived from a frequency shifted version of the transmitted signal. Heterodyning only occurs when the pulsed local oscillator is present so that the local oscillator provides the necessary range gating. Different optical propagation paths may be used to shift the position of the range gate as shown. This system does not require fast detectors. The time resolution is determined by the duration of the local oscillator pulse. The detectors need only respond to the if frequency.

An experiment was carried out to demonstrate this type of imaging. The experiment is shown schematically in Figure 5. The source used was a cw mode locked neodymium-YAG laser that emitted pulses of ~ 100 psec. duration and with a separation of ~ 3 nsec. The beam was expanded to a diameter of ~ 6 cm. and illuminated the target. The polarized component of the return signal was reflected from the Glan-Thompson prism and was shifted in frequency by 40 MHz by an acoustic modulator. It was then heterodyned against a local oscillator derived from the transmitted beam as shown.

The target consisted of a bar holding two retroreflectors that were separated by a distance of 3.5 cm. The target was rotated at 0.5 rps about a horizontal axis. The sweep of the spectrum analyzer was initiated when the bar was at 45° with the upper half receding from the transmitter, and was completed before the target had rotated appreciably. The target was slowly scanned in range, and a spectrum was taken at corresponding points in each revolution. This slow scan in range allowed the various range elements of the signal to be measured sequentially and eliminated

the need for the parallel channels. The resulting signal was displayed on a storage scope. The horizontal position of the beam was scanned in synchronism with the spectrum analyzer sweep and the vertical position was scanned along with the target motion. The output of the spectrum analyzer modulated the beam intensity. This arrangement produced a range-doppler image directly. Such an image is shown in Figure 6. The upper portion shows the results with the laser operating on a single mode (no range resolution) and the lower portion shows the results with the laser mode-locked. The excellent spatial resolution ($\sim$ 2 cm) is evident.

Although this type of signal processing is capable of excellent time resolution, it is inefficient in the use of the received signal energy. Even for the case shown in Figure 4b, where parallel range samples are taken, much of the signal is wasted due to the fact that it must be split among the separate channels for each range element. This is a fundamental problem in any time sampling system. Efficient use of the signal would require some kind of a fast switch or beam deflector to switch the various range elements of the signal to different detectors or it would require a fast detector capable of resolving the time variation of the received signal. As has been mentioned above, the actual information rate of the signal is relatively low so there should exist techniques to process the signals that do not require wide bandwidths. One method is sampling in the frequency domain rather than in the time domain. This type of processing is discussed in detail in the next section. Its success arises from the fact that it is possible to spatially separate the frequency components of an optical signal with a passive device, a spectrometer.

SECTION 2

FREQUENCY DOMAIN SAMPLING

2.1 Analysis

We will first consider the application of frequency domain sampling to the measurement of a repetitive train of extremely fast optical signals. The signal can be represented as a Fourier series

$$S(t) = \sum_{n=N}^{n=N} S_n \cos\left[(\omega_o + n\Omega)t + \varphi_n\right]$$
$$= \begin{cases} s(t)\cos\left(\omega_o t + \Phi(t)\right) & -T/2 \angle 0 \angle T/2 \\ \text{repeats every } T = \dfrac{2\pi}{\Omega} \end{cases} \qquad 2.1$$

The quantities that are to be measured are $s(t)$, the instantaneous amplitude, and $\Phi(t)$, the phase of the signal. It will be assumed throughout that the signal is narrow band in terms of the optical center frequency ω_o, although it may be very wide band in terms of detector capabilities. The Fourier coefficients are given by

$$S_n \sin\varphi_n = -1/T \int_{-T/2}^{T/2} s(t) \sin\left(n\Omega t - \Phi(t)\right) dt$$
$$S_n \cos\varphi_n = +1/T \int_{-T/2}^{T/2} s(t) \cos\left(n\Omega t - \Phi(t)\right) dt \qquad 2.2$$

The general form of the signal processor is shown in Figure 7. The signal is first combined on a beam splitter with a reference waveform. This waveform will be denoted by

$$R(t) = \sum_{n=N}^{n=N} r_n \cos\left[(\omega_o + \omega_1 + n\Omega)\, t + \vartheta_n\right]$$
$$= \begin{cases} r(t)\cos\left[(\omega_o + \omega_1)\, t + \theta(t)\right] & -T/2 \angle 0 \angle T/2 \\ \text{repeats every } T = 2\pi/\Omega \end{cases} \qquad 2.3$$

This reference waveform is periodic with the same period as the original signal, but its optical center frequency is shifted by an amount ω_1. It is assumed that $\omega_1 \angle\angle \Omega \angle\angle \omega_o$. The composite signal leaving the beam splitter is

$$C(t) = \sum_{n=-N}^{n=+N} \left(S_n \cos \left[(\omega_o + n\Omega)t + \varphi_n \right] + r_n \cos \left[(\omega_o + \omega_1 + n\Omega)\, t + \vartheta_n \right] \right) \qquad 2.4$$

The spectrum of this signal is shown schematically in Figure 7. This signal is then passed through a bank of narrow band optical filters. These filters are centered on the lines of the spectrum of C(t). (The lines are actually doublets as shown in Figure 7 , but the spacing of the doublet is small by assumption). The filters will all be assumed to be identical. The transmission of the m th filter for the n th spectral line will be denoted by $T_m(\omega_n)\, e^{i\psi(m,n)}$. Since the filters are identical, the transmission of a given line depends only on its displacement from the center frequency of the filter so that the transmission may be written

$$T(m-n)\, e^{i\psi(m-n)}$$

The cutput of the m th filter is given by

$$F_m = \sum_n T(m-n) \left\{ S_n \cos \left[(\omega_o + n\Omega)\, t + \varphi_n + \psi(n-m) \right] + r_n \cos \left[(\omega_o + \omega_1 + n\Omega)\, t + \vartheta_n + \psi(n-m) \right] \right. \qquad 2.5$$

Each of these outputs is the square law detected to give a signal

$$G_m = \sum_n \sum_{n'} T(n-m)\, T(n'-m) \left\{ S_n \cos \left[(\omega_o + n\Omega)\, t + \varphi_n + \psi(n-m) \right] + r_n \cos \left[(\omega_o + \omega_1 + n\Omega)\, t + \vartheta_n + \psi(n-m) \right] \right\} \cdot \left\{ S_{n'} \cos \left[(\omega_o + n'\Omega)\, t + \varphi_{n'} + \psi(n'-m) \right] + r_{n'} \cos \left[(\omega_o + \omega_1 + n'\Omega)\, t + \vartheta_{n'} + \psi(n'-m) \right] \right\} \qquad 2.6$$

The detectors do not respond at the optical frequency so that only the difference terms in the products of cosines are significant. This gives

$$\bar{G}_m = \frac{1}{2} \sum_{n\,n'} T(n-m)\, T(n'-m) \Big\{ S_n S_{n'} \cos \left[(n-n')\Omega t + \varphi_n - \varphi_{n'} + \psi(n-m) - \psi(n-m) \right]$$

$$+ r_n r_{n'} \cos \left[(n-n')\Omega t + \vartheta_n - \vartheta_{n'} + \psi(n-m) - \psi(n'-m) \right]$$

$$+ S_n r_{n'} \cos \left[(n-n')\Omega t - \omega_1 t + \varphi_n - \vartheta_{n'} + \psi(n'-m) - \psi(n-m) \right] \qquad 2.7$$

$$+ S_{n'} r_n \cos \left[(n-n')\Omega t + \omega_1 t - \varphi_{n'} + \vartheta_{n'} + \psi(n-m) - \psi(n'-m) \right]$$

Each of these signals is now filtered with a narrowband electrical filter centered at ω_1. This eliminates all terms in the above expression except those for which $n' = n$. The resulting signal is

$$H_m = \sum_n T(n-m)^2 S_n r_n \cos (\omega_1 t - \varphi_n + \vartheta_n) \qquad 2.8$$

Here the phase factor of the optical filters has dropped out. Each of these outputs is now multiplied by $\cos (\omega_2 + m\Omega_2)t$ where ω_2 and Ω_2 are chosen at will (but with $\Omega_2 \angle\angle \omega_2$). They are then summed to give

$$W(t) = \frac{1}{2} \sum_n \sum_m T(n-m)^2 S_n r_n \Big\{ \cos \left[(\omega_1 + \omega_2 + M\Omega_2)t - \varphi_n + \vartheta_n \right] \qquad 2.9$$

$$+ \cos \left[(\omega_2 - \omega_1 + M\Omega_2)t + \varphi_n - \vartheta_n \right] \Big\}$$

This may be written in a more convenient form by letting $p = n-m$ and eliminating m. The result is

$$W(t) = \frac{1}{2} \left(\sum_p T(p)^2 \cos p\Omega_2 t \right) \left(\sum_n S_n r_n \cos \left[(\omega_1 + \omega_2 + n\Omega_2)t - \varphi_n + \vartheta_n \right] \right)$$

$$+ \frac{1}{2} \left(\sum_p T(p)^2 \sin p\Omega_2 t \right) \left(\sum_n S_n r_n \sin \left[(\omega_1 + \omega_2 + n\Omega_2)t - \varphi_n + \vartheta_n \right] \right)$$

$$+ \frac{1}{2} \left(\sum T(p)^2 \cos p\Omega_2 t \right) \left(\sum_n S_n r_n \cos \left[(\omega_2 - \omega_1 + n\Omega_2)t + \varphi_n - \vartheta_n \right] \right)$$

$$+ \frac{1}{2} \left(\sum T(p)^2 \sin p\Omega_2 t \right) \left(\sum S_n r_n \sin \left[(\omega_2 - \omega_1 + n\Omega_2)t + \varphi_n - \vartheta_n \right] \right) \qquad 2.10$$

We now consider some special cases. If the filters are sufficiently narrow that they only pass one spectral line, then $T(p) = \delta(p)$ and

$$W(t) = \frac{1}{2}\ \Sigma S_n r_n \cos\ \left[(\omega_1 + \omega_2 + n\Omega_2)\ t - \varphi_n + \vartheta_n\right]$$
$$+ \frac{1}{2}\ \Sigma S_n r_n \cos\ \left[(\omega_1 + \omega_2 + n\Omega_2)\ t + \varphi_n - \vartheta_n\right] \qquad 2.11$$

Suppose now that the reference waveform consists of a train of extremely short pulses. In this case r_n is essentially constant and $\vartheta_n = 0$. We have then

$$W(t) \sim \frac{1}{2}\ \Sigma S_n \cos\ \left[(\omega_1 + \omega_2 + n\Omega_2)\ t - \varphi_n\right]$$
$$+ \frac{1}{2}\ \Sigma S_n \cos\ \left[(\omega_1 - \omega_2 + n\Omega_2)\ t + \varphi_n\right] \qquad 2.12$$

Reference to Eq. 2.1 will show that

$$W(t) = \frac{1}{2}\ S(-\alpha t) \cos\ \left[(\omega_1 + \omega_2)\ t - \Phi\ (-\alpha t)\right]$$
$$+ \frac{1}{2}\ S(\alpha t) \cos\ \left[(\omega_1 - \omega_2)\ t + \Phi\ (\alpha t)\right] \qquad 2.13$$
$$= W_+ (t) + W_- (t)$$
$$\text{for } -T_2/2 \angle 0 \angle T_1/2$$
$$\text{repeating with period } T_2 = 2\Pi/\Omega_2$$
$$\text{and with } \alpha = \frac{\Omega_2}{\Omega}$$

The second term is this an exact replica of the original optical signal but with a time scale that has been stretched by a factor Ω/Ω_2. The center frequency of the signal has also been changed from the optical frequency ω_o to an r.f. frequency $\omega_1 - \omega_2$. The first term is a time reversed version of the optical signal, stretched in time, and with a center frequency $\omega_1 + \omega_2$. The signal processor has extracted the amplitude and phase of each of the componets of the line spectrum of the original optical signal and has imposed them on a line spectrum at an r.f. frequency. This synthesizes the original signal. The signal and its time reversed version may be readily separated by the proper choice of ω_1 and ω_2 together with frequency filtering.

Let us now consider the more general case where r_n and ϑ_n are arbitrary. The component at $\omega_2 - \omega_1$ is

$$W(t) = \frac{1}{2}\ \Sigma S_n r_n \cos\ \left[(\omega_1 - \omega_2 + n\Omega_2)\ t + \varphi_n - \vartheta_n\right] \qquad 2.14$$

The cross correlation of the signals s(t) and r(t) is

$$\int_{-T/2}^{T/2} S(t)\mathbf{R}(t-\tau)dt = \frac{T}{2} \sum_n S_n r_n \cos \left[(\omega_o + n\Omega)\,\tau + \varphi_n - \vartheta_n\right] \quad 2.15$$

The function $W_-(t)$ may be seen to be a repetitive time display of the cross correlation function. The function $W_+(t)$ is just a time reversed version of this signal. In the case where S(t) and R(t) are identical, the processor gives the autocorrelation function as a function of time; i.e., it behaves as a matched filter. In the case where R(t) is a train of pulses of finite duration pulses rather than extremely narrow pulses, the original signal is received with a degraded time resolution given by the duration of the pulses constituting R(t).

We may now return to the more general case given in Eq. 2.10. Let

$$\begin{aligned} \sum_p T(p)^2 \cos p\Omega_2 t &= T_c(t) \\ \sum T(p)^2 \sin p\Omega_2 t &= T_s(t) \end{aligned} \quad 2.16$$

We note that if the bandpass of the optical filters are symmetric; i.e., if $|T(p)| = |T(-p)|$, then $T_s(t) = 0$.

$$\begin{aligned} G(t) &= \Sigma\, s_n r_n \cos \left[(\omega_1 + \omega_2 + n\Omega_2)\, t - \varphi_n + \vartheta_n\right] \\ &= g(t) \cos \left[(\omega_1 + \omega_2)\, t + \gamma(t)\right] \quad 2.17 \\ &\quad \text{(periodic at } T_2 = 2\pi/\Omega_2) \end{aligned}$$

For a narrowband waveform, it will be true that

$$\sum S_n r_n \sin \left[(\omega_1 + \omega_2 + n\Omega)\, t - \varphi_n + \vartheta_n\right] = g(t) \sin \left[(\omega_1 + \omega_2)\, t + \gamma(t)\right] \quad 2.18$$

So that we have for the $\omega_1 + \omega_2$ component of Eq. 2.10

$$W_+ = T_c(t)\, g(t) \cos \left[(\omega_1 + \omega_2)\, t + \gamma(t)\right] + T_s(t) g(t) \sin \left[(\omega_1 + \omega_2)\, t + \gamma(t)\right] \quad 2.19$$

A similar expression holds for W_-. The shape of the filter transmission function multiplies the output of the system by a known function of time. The result that would be obtained with very narrow filters can be computed from the result obtained from wider filters. Alternately, the filter functions could be chosen to perform additional signal processing operations.

The entire discussion above has assumed that the pulse train is strictly periodic. If the signal is a return from a moving target, it will not be periodic but will change gradually with a time characteristic of the reciprocal of the doppler spread. If the scaling in time is chosen so that the new, expanded repetition period is less than the reciprocal of the doppler spread, then the reconstructed signal will faithfully follow the variations of the original signal due to the dappler spread.

The entire discussion above has been concerned with repetitive signals. The frequency domain sampling technique is not restricted to this case. It may be applied to the measurement of a single optical transient. The processing is somewhat more complicated in this case because it corresponds to heterodyning with zero difference frequency and care must be taken to avoid spectral overlapping. A system to perform this measurement is illustrated schematically in Figure 9. We assume again a signal and a reference

$$S(t) = \frac{1}{(2\pi)^{\frac{1}{2}}} \int e^{+i\omega t}\, s(\omega)\, d\omega$$

$$R(t) = \frac{1}{(2\pi)^{\frac{1}{2}}} \int e^{i\omega t}\, r(\omega)\, d\omega \qquad 2.20$$

The signals are combined on a beamsplitter to produce a composite spectrum

$$c(\omega) = s(\omega) \pm r(\omega) \qquad 2.21$$

The two signs are obtained from opposite sides of the beamsplitter. The composite signal is then passed through a filter bank. At the output of each filter a signal

$$\underset{m}{F}(\omega) = R\left(S(\omega) \pm r(\omega)\right) T_m(\omega) \qquad 2.22$$

is obtained. This is square law detected and integrated over time to obtain

$$G_m = \int_{-\infty}^{\infty} \left|s(\omega) \pm r(\omega)\right|^2 \left|T_m(\omega)\right|^2 d\omega \qquad 2.23$$

$$= \int_{-\infty}^{\infty} \left\{ \left|s(\omega)\right|^2 \pm \mathrm{Re}\left(r(\omega)s^*(\omega)\right) + \left|r(\omega)\right|^2 \right\} T_n(\omega)\, d\omega$$

The difference between the plus and minus signals is then taken to give

$$U_m = 2 \int_{-\infty}^{\infty} \mathrm{Re}\left(r(\omega)s^*(\omega)\right)\, T_m(\omega)\, d\omega \qquad 2.24$$

If the filters are extremely narrow, $T_n(\omega) \approx \delta(\omega-\omega_m)$ and

$$U_m = 2\ \mathrm{Re}\left(r(\omega_m)\, s^*(\omega_m)\right) \qquad 2.25$$

If the same operation is repeated with the reference wave shifted by $\lambda/4$, the output

$$U_m' = 2\ \mathrm{Im}\left(r(\omega_m)\, s^*(\omega_m)\right) \qquad 2.26$$

will be obtained. We thus obtain a sampled version of $r(\omega)\, S^*(\omega)$. This quantity is the Fourier Transform of the cross correlation function; i.e.

$$\int_{-\infty}^{\infty} R(t)\, S\,(t-\tau)\, dt = \int_{-\infty}^{\infty} e^{i\omega t}\, r(\omega)\, s^*(\omega)\, d\omega \qquad 2.27$$

These parallel outputs may be used to reconstruct the signal at any desired frequency and repetition rate in a manner identical to the previous discussion.

2.2 Discussion and Experimental Implementation

The analysis of the previous section described the operation of the frequency sampler in the time domain. Figure 8 shows the situation in the frequency domain, and illustrates why the turn frequency domain sampling has been used. The various components of the line spectra of R(t) pass through the filters, are isolated, and are distributed to separate detectors. If an appropriate local oscillator were available at each detector, the amplitude and phase of each of the components could be measured. This would completely characterize the signal. Just such a set of local oscillators can be obtained by filtering a periodic train of short pulses through the same filter bank as the signal. Each channel can be operated in the quantum noise limited regime, and all of the energy received in each channel is used.

An alternate way of looking at the operation of the system is to consider the response of one of the narrow band filters to a short optical pulse. The output of the filter has a duration corresponding to the reciprocal of the bandwidth of the filter. This should be made comparable to the duration of the signal that is to be measured. The reference signal can thus heterodyne with the signal over its entire duration. The precise details of the resulting signal are given above.

We may now consider means of implementing such a detection system. One of the first considerations is the resolving power required of the filters. Let us assume that the line shape of the filter is

$$T_{(p)} = \frac{\sin \alpha p}{\alpha p} \tag{2.28}$$

where the first zeros occur at $\alpha p = \pm \pi$. The modulating functions are

$$T_s(t) = 0$$

$$T_c(t) = \sum_{p=-P}^{p=P} \frac{\sin^2 \alpha p}{(\alpha p)^2} \cos p\Omega_2 t \tag{2.29}$$

This is a periodic function with period $T_2 = 2\pi/\Omega_2$. We may rewrite this in the form

$$T_c(t) = \frac{1}{\alpha^2} + \frac{2}{\alpha^2} \sum_{p=1}^{p=P} \frac{\sin^2 \alpha p}{p^2} \cos p\Omega_2 t \tag{2.30}$$

For values of $\alpha < \pi$ this simply represents a triangular pulse extending from $-\alpha/\Omega < t < \alpha/\Omega$ as shown in Figure 10. When $\alpha = \pi$ the pulse extends over the entire interval $-T/2 < t < T_2/2$. For larger values of α, the base line lifts as shown in the figure. For the particular values $\alpha = R\pi$, the function $T_c(t) = 1$. The reason for this is shown in Figure 10. Although the filter has finite transmission off its center frequency, its transmission for the lines of the spectrum of S(t) is zero except for the line on center.

For ease in data interpretation, the filters should be made quite narrow (or they should satisfy the condition illustrated in Figure 11). They should not, however, be made so narrow that they are capable of resolving the if frequency, since this will pervent the heterodyning of the signal and the reference waveforms. The bandwidth $\Delta\omega$ of the filters should be in the range $\omega_{if} < \Delta\omega < \Omega$. For a typical mode locked laser, $\Omega/2\pi \sim 3 \times 10^8$ Hz, at a wavelength of 1.06 μ, $\omega_o/2\pi = 3 \times 10^{14}$ Hz. This corresponds to a resolving power of $\omega_o/\Delta\omega \sim 10^6$. This resolving power is easily obtainable with a Fabey-Perot etalon. It can be obtained with more difficulty with a grating, a large grating, possibly with several passes would be required. The grating approach, however, has several advantages which will be discussed later.

The number of filters required is determined by the desired time resolution (which is ultimately determined by the bandwidth of the reference signal). Figure 12 shows the response of the system to an amplitude step for a filter bank employing 5, 11 and 21 filters. Figure 13 shows the amplitude and phase of the response of the system to a pulse of constant amplitude and linearly increasing phase (a frequency offset) for a filter bank with 11 components, and Figure 14 for one with 21 components. Figure 15 shows the response to a chirped pulse for 11 and 21 components. These responses were computed by calculating the Fourier coefficients of the applied waveform, truncating them at the desired number of components and then reconstructing the series with the truncated set of coefficients.

The problems involved in the experimental demonstration of the frequency domain sampling technique are:

1. attainment of sufficient resolving power in the optical filter bank
2. simultaneous detection of the signals from each of the filters
3. modulation of the output of each detector by the appropriate modulation waveform
4. recombination of the modulated outputs to regenerate the time-scaled version of the original signal.

The first of these requirements determines the type of spectrometer that is required. The spectrometer must have:

1. a resolving power of the order of 10^6
2. high throughput
3. produce an output of all the frequency components of the incident beam simultaneously.

A Fabry Perot etalon can satisfy the first two of these requirements readily. It does not, however, satisfy the third. When a Fabry Perot etalon is operated with a collimated input beam, it acts as an optical band pass; i.e., it passes the wavelength to which it tuned, with high transmission, and it reflects all the other wavelengths with low loss. If it is operated with an input beam from an extended source or one with more divergence than the diffraction limit of its aperture, then it acts as a spectrometer and produces the characteristic circular fringe pattern. This, however, entails a loss of signal power. A plane Fabry Perot basically provides a transmission that depends on the angle of propagation of the beam with respect to the normal to the reflectors. It has a high throughput for components at the proper frequency and angle. The best that can be done is to arrange the divergence of the input beam so that only one free spectral range is illuminated. The total power transmitted in a given ring is then given by the total power incident at the frequency corresponding to the ring divided by the finesse of the interferometer.

The ease with which a high resolving power can be obtained with a Fabry Perot etalon makes it attractive, however, and it will be used for a demonstration of the frequency domain sampling technique.

The most convenient form of spectrometer for use in the system is a grating. Grating can have a high throughput and produce a spatially disfused output at all frequencies simultaneously. The main problem is that of obtaining sufficient resolution. Conventional gratings are limited to a resolution of the order of 500,000. Echelle gratings are capable of resolutions in the range of 500,000 to 2,000,000. For any type of multiple beam dispersive device, the resolution will be determined by the difference in transit time between the shortest and the longest path in the device; i.e.,

$$\Delta f \sim \frac{1}{\Delta \tau}$$

and

$$R = \frac{f}{\Delta f} = f \, \Delta \tau \qquad (2.31)$$

For a grating used in a Littrow arrangement as shown in Figure 15,

$$\Delta\tau = \frac{2\,W \sin\alpha}{c}$$

and

$$R = \frac{2\,W}{\lambda} \sin\alpha \tag{2.32}$$

Echelle gratings are typically operated with a diffraction angle $\alpha \sim 65^{\circ}$ so that $\sin\alpha \approx 0.9$. Thus to achieve a resolution of 10^6 at a wavelength of 1 micron, a grating of width

$$W = \frac{\tau\,R}{2 \sin\alpha} = 55 \text{ cm} \tag{2.33}$$

is required. This is an impractically large size for a single grating. The required resolution may be obtained by multiple diffractions. Two-pass and four-pass instruments have been fabricated and operated successfully. For a four-pass instrument the grating width is reduced to 14 cm, a size that is commerically obtainable at reasonable cost.

The required resolution for the frequency domain sampling system is obtainable easily with a Fabry Perot filter and with more difficulty with an echelle grating. We must now turn to the problem of performing the required signal processing after the dispersion is obtained. One means of performing this would be to implement the system exactly as shown in Figure 7. The output of the grating could be imaged upon a close packed array of detectors, one for each resoluable frequency element. The output of each detector could then be modulated in an electronic mixer with the appropriate modulation frequency and the results summed electronically to yield the desired output. There is no fundamental objection to this approach except for the difficulty involved in maintaining balance among all the separate channels and the large number of separate electronic channels that are needed.

Fortunately, the entire signal processing operation after dispersion can be conveniently and simply accomplished by a parallel optical processor. We consider an alternate form of the signal processes as shown in Fig. 17. In this form the modulators operate on the optical signals prior to detection. Both the signal and the reference are modulated. If the modulating function is $f_m(t)$, then the quantity H_m of Eq. (2.8) becomes

$$Hm' = Hmfm^2(t). \tag{2.34}$$

After modulation, the signals are all brought together on a common detector. The resulting output is

$$W'(t) = \tfrac{1}{2} \sum_n \sum_m T(n - m)^2 \, s_n r_n \cos (\omega_1 t - \varphi_n + I_n) \, f_m^{\,2}(t). \quad (2.35)$$

If we take

$$f_m(t) = \cos \tfrac{1}{2}(\omega_2 + m\Omega_2)t, \quad (2.36)$$

then,

$$f_m^{\,2}(t) = \cos^2 \tfrac{1}{2}(\omega_2 + m\Omega_2)t = \tfrac{1}{2}\left[1 + \cos (\omega_2 + m\Omega_2)t\right]. \quad (2.37)$$

The components of $W'(t)$ at $\omega_2 \pm \omega_1 + m\Omega$ are identical to those of $W(t)$ of Eq. (2.10). There is an additional component at ω_1, however, this may be removed by electrical filtering. One need only choose ω_2, m and Ω so that these components do not overlap. This form of the signal processor is attractive becuase it eliminates the need for multiple detectors and allows the use of a simple technique to perform all of the modulation operations in parallel. This technique makes use of a special chopper in conjunction with a Fabry-Perot interferometer. This technique has been used by Hirschberg, et at (Ref. 1) a different purpose, a frequency multiplexed Fabry-Perot for investigation of spectral line shapes. Although the Fabry-Perot is not the optimum dispersive element, it was used for an experimental demonstration and the basic idea of the technique can be extended to other dispersive devices.

The fringe pattern that would be obtained from a Fabry-Perot interferometer that is illuminated by a line spectrum is shown in Fig. 18. (For clarity, only four lines are shown, and in reality, each line would be in overlapping doublet consisting of the signal and reference lines). The laser pattern of the figure shows one free spectral range of the interferometer. We now want to modulate each of the these rings with a different modulation frequency. This can be accomplished by the so called multizone disk modulator (Ref. 1). The disk is shown schematically in Fig. 19. It consists of a transparent substrate that is divided into a number of annular zones. The mean radius of each zone is centered on one of the rings that are observed in the focal plane of a Fabry-Perot interferometer. Each zone is divided into an equal number of transparent and opaque areas and the number of such areas increased as the radius of the zone increases. Two such disks are placed in the plane of the Fabry-Perot

Ref. 1 J. G. Hirshberg, W. I. Fried, L. Hazelton, Jr. and A. Wouters Appl. Opt. 8, 1979 (1971)

fringes and one is rotated with respect to the other. Each of the lines of the spectrum is thus chapped at a different frequency determined by the number of "teeth" in the zone on which it falls and the rotation rate. This modulator performs very nearly the required operation. The modulating functions are triangular waves rather than square waves, but if we arrange the lowest modulating frequency to the breater than $\frac{1}{2}$ of the highest frequency, then all the higher harmonics of the modulation waveform can be filtered out electrically.

The multiplexing scheme used with the Fabry-Perot can be applied to other types of dispersive elements such as an echelle grating. A possible arrangement is shown in Fig. 20. The output of the grating is focused in the direction normal to the dispersion by a cylindrical lens. This line is then scanned by a beam deflector across a mesh whose transparency is shown schematically in the figure. The signal transmitted through the mask is then focused into a detector. In addition to eliminating the inefficiency associated with the Fabry-Perot, this scheme is capable of modulating at much higher frequencies. The modulation frequency is limited only by the speed of the beam deflector which may be mechanical, electrooptical or acousto-optical.

A multizone disc has been fabricated for use with a Fabry-Perot interferometer. It is illustrated in Fig. 21. It consists of 50 annular zones of equal area. The innermost zone has 50 light and 50 dark areas. The number of transparent and opaque areas increases by one with each zone out to the outermost zone which has 99. This disk was drawn on a large numerically controlled drafting machine at 25 times final size. The pattern was then photographically reduced onto a glass disk having the dimensions indicated on the figure. When driven with a 400 Hz synchronous motor, the disk provides a comb of modulation frequencies that range from 20 to 40 kHz in steps of 400 Hz. A stationary disk was mounted in close proximity to the rotating disk and was provided with an x-y pace timing adjustment. Centering of the disks relative to one another was accomplished by projecting a beam of light through the disks and observing the Moire pattern produced on a screen. When the disks are centered, the pattern consists of circular rings that expand or contract symmetrically as the disks are slowly rotated. The centering of the rotating disk on the driving shaft was done under a microscope.

The radii of the zones on the disk were chosen to correspond to equally spaced frequency increments on a Fabry-Perot interference pattern. The condition for a maximum in the transmission of a Fabry-Perot of spacing d is

$$m \lambda = 2d \cos \theta \qquad (2.38)$$

where m is the order of interference on the axis. If we have a maximum on the axis, then the next maximum will occur at

$$(m - 1)\lambda = 2d \cos \theta_1 \tag{2.39}$$

or

$$\left(\frac{\lambda}{2d}\right) = 1 - \cos \theta_1 \approx 1 - \left(1 - \frac{\theta_1^2}{2}\right)$$

$$= \frac{\theta_1^2}{2} . \tag{2.40}$$

For the present case, it was more convenient to have a dark fringe in the center. This condition corresponds to

$$(m + \tfrac{1}{2})\lambda = 2d \cos \theta = 2d . \tag{2.41}$$

The first maximum will occur when

$$m\lambda = 2d \cos \theta_1 \tag{2.42}$$

and the next maximum when

$$(m - 1)\lambda = 2d \cos \theta_2 . \tag{2.43}$$

This gives

$$\tfrac{1}{4}\frac{\lambda}{d} = 1 - \cos \theta_1 \approx \frac{\theta_1^2}{2}$$

$$\left(\frac{\lambda}{2d}\right) = \theta_1^2 \tag{2.44}$$

and for the next maximum

$$3/4\,\frac{\lambda}{d} = 1 - \cos\theta_2 \approx \frac{\theta_2^2}{2}$$

$$\frac{3\lambda}{2d} = \theta_2^2 = 3\,\theta_1^2 \qquad (2.45)$$

$$\theta_2^2 = \sqrt{3}\;\theta_1^2.$$

This relation determines the ratio between the angles corresponding to one free spectral range of the interferometer. In the experiment, a spacing of 0.5 cm was used, corresponding to a free spectral range of 30 GHz. This then determines

$$\theta_1^2 \approx 10^{-4} \qquad \text{at } \lambda = 10^{-4} \text{ cm}$$

$$\theta_1 = 10^{-2} \qquad (2.46)$$

$$\theta_2 = 1.732 \times 10^{-2}.$$

The radius of the rings in the Fabry-Perot pattern will be given by $F\theta$ where F is the focal length of the lens used to image the rings in the focal plane. For a 1 m focal length, this determines R_1 = 1 cm and R_2 = 1.732 cm. These were the dimensions that were chosen for the inner and outer radii of the multizone disc modulator. Differentiating the formula,

$$m = \frac{2d}{c} f \cos\theta. \qquad (2.47)$$

We find

$$df = \frac{\sin\theta}{\cos\theta}\,d\theta \approx \sin\theta\, d\theta. \qquad (2.48)$$

So that if we observe the interference rings at the focal plane of a lens of length F, the range of frequencies falling in an area

$$dA = rdr = F^2 \sin\theta\, d\theta = F^2 df$$

i.e., annular rings of equal area correspond to equal frequency intervals. The multizone disk was divided into 50 annular rings of equal area. The inner radius and outer radius of the n^{th} ring are given by

$$\begin{aligned} r_{inner} &= [1 + 0.04(n - 1)]^{\frac{1}{2}} \text{ cm} \\ r_{outer} &= [1 + 0.04(n)]^{\frac{1}{2}} \\ \pi r_o^2 - \pi r_i^2 &= 0.04\,\pi \text{ cm}^2 \end{aligned} \tag{2.49}$$

Each ring of the modulator thus corresponded to a frequency increment of 30 GHz/50 = 600 MHz. In order to match up the line spectrum of the laser with the disk, the laser should then be operated at a mode spacing frequency of 600 MHz. It was found, however, that deviations from this condition did not seriously degrade the operation of the system.

The multizone disk modulator was used to demonstrate the operation of the frequency domain signal processor. The complete arrangement is shown in Figs. 22 and 23. Figure 22 shows the optical layout. The beam emerges from the laser, and a small portion is split off to serve as a local oscillator. The remainder is sent to the target and, on its return, is shifted by 40 MHz by an acousto-optic modulator. It is combined with the local oscillator on a beam splitter. The output from one side of the beam splitter is sent to an auxiliary detector to allow wavefront alignment prior to further processing of the signal. This is most conveniently done by operating the laser in a single, or at most a few longitudinal modes. This can be done by turning off the mode-locking modulator and placing an etalon in the cavity. The aligned signal and local oscillator beams are then passed through a diverging lens to allow the illumination of approximately one free spectral range of the interference pattern. A cylindrical lens was used rather than a spherical lens since it allows more of the signal to be used. The cylindrical lens illuminates a stripe across the pattern rather than the entire ring pattern. The beams then passed through an angular and translational alignment element to allow optimum positioning of the beams. They then passed into a high resolution Fabry-Perot interferometer. The unit used was a Burleigh Model RC40. It had a mirror figure of $\lambda/200$ and a mirror reflectivity of $R_1 = R_2 = 98.5\%$. The output from the interferometer was then focused by a 1 m lens in the multizone disk modulator. Care was taken to center the ring pattern (produced with a spherical diverging lens) on the multizone disk. After modulation, the signal was collected and focused into a PIN diode detector (EG&G YAG 100) which was connected to a low noise preamplifier tuned to 40 MHz.

The electrical circuit for the system is shown in Fig. 23. A 40 MHz oscillator is used to drive the acousto-optic modulator. A portion of this signal, with variable amplitude and 2π phase control is added to the output of the PIN diode to cancel any feedthrough of the 40 MHz signal. (Feedthrough is virtually impossible to eliminate, but may be easily cancelled as was done here. The presence of a large feedthrough signal can result in saturation of other elements in the circuit). The resulting signal, may then be displayed on a spectrum analyzer. The signal at this point consists of a component at 40 MHz corresponding to the dc component of the triangular waveforms from the multizone disk modulator, a band of components at 40.020 to 40.040 MHz corresponding to the $\omega_2 + \omega_1$ components of Eq. (2.10) and a band of components at 39.060 to 39.080 corresponding to the $\omega_2 - \omega_1$ components of Eq. (2.10). This signal is then sent to a radio receiver which can be tuned to either of the sideband components. The output is taken from the final IF frequency at 80 kHz. This signal is then displayed on an oscilloscope. A synchronizing signal is taken from the oscillator that drives the multizone disk modulator so that the sweep of the scope is synchronized to the 400 Hz fundamental repetition rate of the modulator.

2.3 Experimental Results

The system described above performed extremely well and has demonstrated all of the features of the frequency domain processor. In the test to be described here, a plane mirror was used as the target. The upper pattern of Fig. 24 shows the spectrum of the transmitted signal as measured with an auxiliary scanning Fabry-Perot with a free spectral range of 8 GHz. The lower portion shows the reconstructed waveform that was obtained from the system. The interpulse spacing has been expanded in time to 2.5 μsec from $\sim$ 2 nsec. By varying the amplitude of the mode-locking modulator drive on the laser, the oscillating line width of the laser could be varied and the corresponding variation in the reconstructed pulse width could be observed. This is illustrated dramatically in Fig. 25. The upper portion of the figure shows the transmitted spectrum. In this case the bandwidth of the laser was restricted to 2-3 modes by an etalon. The lower portion shows the reconstructed pulse train. The narrow pulses of Fig. 24 have been broadened to a nearly sinusoidal modulation by the reduction inthe laser bandwidth. A similar effect may be produced by masking off portions of the fringe pattern that is incident on the multizone disk modulator. This reduces the bandwidth of the reconstructed waveform and results in a broadening of the pulses.

Figures 26 to 28 show the time reversal feature of the frequncy domain processor. The target used in this case was a pair of mirrors as shown in Fig. 26. The mirrors were slightly misaligned to prevent multiple reflections so that the return consisted of two closely spaced pulses. Figure 27 shows the reconstruction of the signal received from this target. The signal was reconstructed using the lower sideband (39.060 - 39.080 MHz) of the received signal. Blocking the second mirror produced the signal shown in the lower portion of the figure. The second pulse of the pair in the upper portion of the figure thus corresponds to the return from the most distant mirror. Using the same target, the signal was reconstructed from the upper (40.020 - 40.040 MHz) sideband of the detected signal (by retuning the radio). The results are shown in Fig. 28. Blocking of the furthest mirror now eliminates the first of the pair of pulses, illustrating the time reversal discussed in the previous section.

In most of the photographs a smaller pulse may be observed halfway between the large pulses in the reconstructed pulse train. This pulse is not present in the optical signal; it is an artifact of the reconstruction process. It arises because the ring pattern from the Fabry-Perot is not precisely registered on the multizone disk and because the mode spacing of the laser was not exactly equal to the design frequency spacing of the annular regions on the multizone disk modulator (600 MHz). The laser was actually operated with a mode spacing of approximately 475 MHz. This difference leads to a misregistration of the modes on the disk and results in cross talk between adjacent modes in the reconstructed signal. The main effect of this is to produce spurious signals at one half of the basic pulse spacing. The amplitude of this spurious signal was sensitive to the alignment and finesse of the interferometer and to small changes in the interferometer length. The spurious signals can presumably be eliminated by more careful matching of the laser mode spacing and the multizone disk modulator.

Appendix I

The following is a list of publications and major presentations for which partial or complete support can be attributed to the present contract.

1. G. L. Lamb, Jr., "Propagation of Ultrashort Optical Pulses," Phys. Letters 25A, 181 (1967).

2. G. L. Lamb, Jr., Lecture at Summer School in Quantum Electronics held at Flagstaff, Arizona, June 17-28, 1968.

3. M. E. Mack, "Measurement of Nanosecond Flucrescent Decay Lines," J. Appl. Physics 39, 2483 (1968).

4. M. E. Mack, "Light Amplification in Saturable Absorbers," Appl. Phys. Letters 12, 329 (May 15, 1968).

5. M. E. Mack, "Recovery Time and Non-Linearities in Bleachable Absorbers," presented at the 1968 International Quantum Electronics Conference, Miami, Florida (May 14-17, 1968).

6. M. E. Mack, "Light Amplification in Saturable Absorbers," presented as a post deadline paper at the 1968 International Quantum Electronics Conference, Miami, Florida (14-17, 1968).

7. M. J. Brienza, A. J. DeMaria, and W. H. Glenn, "Optical Rectification of Mode-Locked Laser Pulses," Phys. Letters 26A, 390 (1968).

8. M. J. Brienza, A. J. DeMaria and W. H. Glenn, "Optical Rectification of Mode-Locked Laser Pulses" presented at the 1968 International Quantum Electronics Conference, Miami, Florida (May 14-17, 1968).

9. W. H. Glenn, M. J. Brienza, A. J. DeMaria, "Mode-Locking of an Organic Dye Laser," Appl. Phys. Letters 12, 54 (1968).

10. A. J. DeMaria, "Nonlinear Optical Studies with Picosecond Light Pulses," (Invited) A.P.S. March Meeting in Berkeley (March 18-21, 1968).

11. A. J. DeMaria, "Nonlinear Interaction of Subnanosecond Light Pulses," (Invited) Optical Society of America, Washington, D.C. (March 13-16, 1968).

12. W. H. Glenn, "Generation and Measurement of Picosecond Pulses," (Invited) A.P.S. February Meeting in Boston (Feb. 26-28, 1968).

13. A. J. DeMaria, "Picosecond Laser Pulses," E.E. Seminar, Ohio State University (March 1968).

14. A. J. DeMaria, "Generation Measurement and Utilization of Picosecond Laser Pulses," (Invited) M.I.T. Lincoln Laboratory (Feb. 14, 1968).

15. A. J. DeMaria, "Picosecond Laser Pulses," Physics Seminar, Bell Telephone Laboratories, Holmdel, N.J. (January 1968).

16. W. H. Glenn, "Generation and Measurement of Properties of Picosecond Laser Pulses," (Invited) Fall 1967 URSI and IEEE G-AP Meetings (October 16-19, 1967).

17. A. J. DeMaria, "Ultrashort Light Pulses," (Invited) NEREM, Boston, Massachusetts (October, 1967).

18. A. J. DeMaria, Lecture at Summer School in Quantum Electronics held at Flagstaff, Arizona (June 17-28, 1968).

19. M. E. Mack, "Measurement of Nanosecond Fluorescent Decay Times," Conference on Subnanosecond Light Pulses, Durham, North Carolina (November 14-17, 1967).

20. G. L. Lamb, Jr., "Optical Pulse Propagation in an Inhomogeneously Broadened Medium" Phys. Letters 28A p 548 Jan. 1969.

21. E. B. Treacy, "Generation of Chirped Pulses at 10.6 Microns Wavelength" Proc. IEEE 56 p 2053-2054 November 1968.

22. E. B. Treacy "Adiabatic Inversion with Light Pulses" Phys. Letters 27A pp 421-422 August 1968.

23. M. E. "Stimulated Thermal Light Scattering in the Picosecond Regime" Phys. Rev. Letters 22 13 January 1969.

24. A. J. DeMaria, W. H. Glenn, M. J. Brienza and M. E. Mack, "Picosecond Laser Pulses" (invited paper) Proc. IEEE 57 p. 2-25 January 1969.

25. E. B. Treacy, Chirped Optical Pulses, Annals of the New York Academy of Sciences 168, 400 - 418, 1970.

26. M. E. Mack, Stimulated Thermal Rayleigh Scattering with Picosecond Pulses, Annals of the New York Academy of Sciences, 419 - 436, 1970.

27. E. B. Treacy, Measurement of Phase Structure in Picosecond Pulses, S minar presented at the University of Rochester, Department of Physics, December 8, 1969.

28. M. E. Mack, R. L. Carman, F. Shimizu, and N. Bloembergen, Forward Picosecond Stokes Pulse Generation in Transient Stimulted Raman Scattering, Phys. Rev. Letters 23, 1327 (1969).

29. M. E. Mack, Superradient Traveling Wave Dye Laser, Appl. Phys. Letters 15, 166 (1969).

30. W. H. Glenn, Picosecond Laser Pulses, Seminar presented at the Summer School in Quantum Electronics, University of Colorado, Boulder, Colorado, August 14, 1969; Picosecond Laser Pulses, Am. Phys. Soc. DEAP Meeting, Washington, D.C., May 2, 1969.

31. E. B. Treacy, Lectures on mode-locked lasers, measurement of picosecond pulses and optical adiabatic inversion presented at the Physics of Quantum Electronics Summer School, Flagstaff, Arizona, June, 1969.

32. M. E. Mack, and E. B. Treach, Nonlinear Effects in the Propagation of Picosecond Pulses, Spring Meeting of the New England Section of the American Physical Society, Storrs, Connecticut, April 12, 1969.

33. E. B. Treacy, and A. J. DeMaria, Adiabatic Inversion of SF_6 in the Infrared, Spring Meeting of the New England Section of the American Physical Society, Storrs, Connecticut, April 12, 1969.

34. M. E. Mack, R. L. Carman, J. Rientjes and N. Bloembergen, Transient Stimulated Rotational and Vibrational Scattering in Gases, Appl. Phys. Letters 16, 209, (1970).

35. C. M. Ferrar, Simple, High Intensity, Short Pulse Flashlamps, Rev. Sci. Instr. 40, 1436 - 1438 (1969).

36. C. M. Ferrar, Mode-Locked, Flashlamp Pumped Coumarin Dye Laser at 4600 , IEEE J. Quant. Elect QE-5, 550 (1969).

37. G. L. Lamb, Jr., P_1 Pulse Propagation in a Lossless Amplifier, Phys. Letters 29A, 507 (1969).

38. M. E. Mack, and E. B. Treacy, A Nonlinear Image Contrast Amplifier, IEEE J. Quant. Elect. QE-5, 382 - 383 (1969).

39. E. B. Treacy, and A. J. DeMaria, Adiabatic Inversion in the Infrared, Phys. Letters 29A, 369 - 370 (1969).

40. M. E. Mack, "Bleachable Dyes", presented as an invited paper at the 1970 General Motors Research Conference on the Physics of Opto-Electronic Materials, Warren, Michigan.

41. R. L. Carman, M. E. Mach and J. Reintjes, "Self Trapped Filaments in Gases and Liquids Created from Trains of Picosecond Pulses".

42. R. L. Carman, F. Shimizu, J. Reintjes, N. Bloembergen and M. E. MAck, "Stimulated Raman Scattering in the Picosecond Time Regime".

43. E. B. Treacy, "Pulse Compression and Dynamic Spectroscopy", (Invited Paper). This paper and the preceeding two papers were presented at the 1970 International Quantum Electronics Conference, Kyoto, Japan.

44. G. L. Lamb, Jr., and M. O. Scully, "Higher Conservation Laws for Ultrashort Optical Pulse Propagation in an Inhomogeneously Broadened Medium", presented at the New York Meeting of the American Physical Society, 1-4 February 1971.

45. G. L. Lamb, Jr., "Analytical Descriptions of Ultrashort Optical Pulse Propagation", Reviews of Modern Physics, 43, 99-124, April 1971.

46. G. L. Lamb, Jr., "Higher Conservation Laws in Ultrashort Optical Pulse Propagation", Physics Letters, 32A, 251-252, 27 July 1970.

47. E. B. Treacy, "Picosecond Light Pulses", Colloquium presented at the Physics Department, University of Queensland, Queensland, Australia, September 25, 1970.

48. M. E. Mack, "Ultrafast Rise-Time Flashlamp For Dye Laser Pumping", Paper 1.5 Conference in Laser Engineering and Applications (CLEA), Washington, D.C. June 2-4, 1971.

49. A. J. DeMaria, W. H. Glenn, M. E. Mack, "Ultrafast Laser Pulses", Physics Today, 24, 19-26, July 1971.

50. W. H. Glenn, "Transient Nonlinear Effects in the Propagation of High Power Laser Beams". Conference on Electron, Ion and Laser Beam Technology, Boulder, Colorado, May 1971.

51. W. H. Glenn, "Ultrashort Pulse Phenomena", presented at the Conference on Solid State Physics, Florida Atlantic University, Boca Raton, Florida, January 7, 1971.

52. W. H. Glenn, "Physics of Picosecond Pulses", Northeastern University, Department of Continuing Education, January 12, 1971.

53. A. R. Clobes and M. J. Brienza, "Single-Frequency Traveling-Wave ND: YAG Laser, Applied Physics Letters

54. W. H. Glenn, "Synthetic Aperture Optical Radar Techniques" to be presented at the 1974 Spring Meeting of the Optical Society of America, 22-25 April, 1974 (Invited)

FIG. 1

RANGE–DOPPLER IMAGING

a)

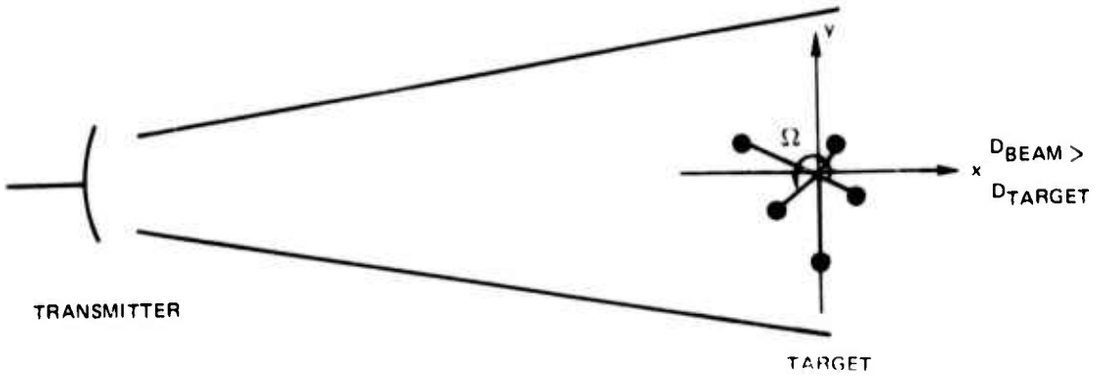

b)

RANGE–DOPPLER IMAGE

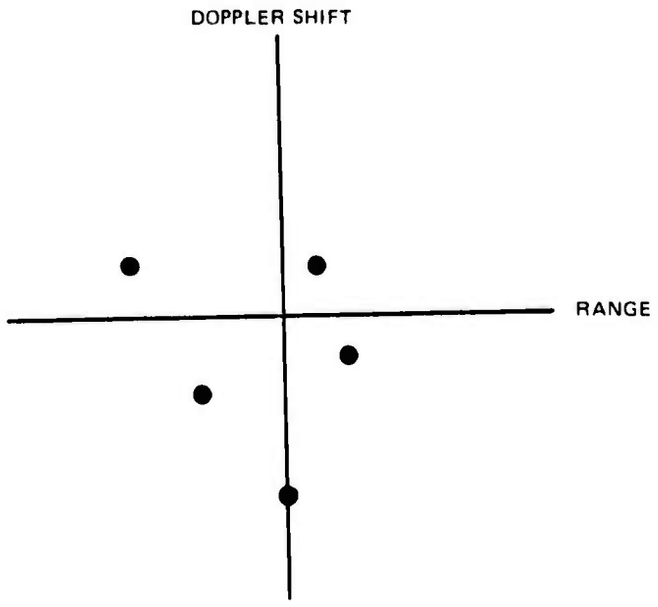

TIME DOMAIN DESCRIPTION

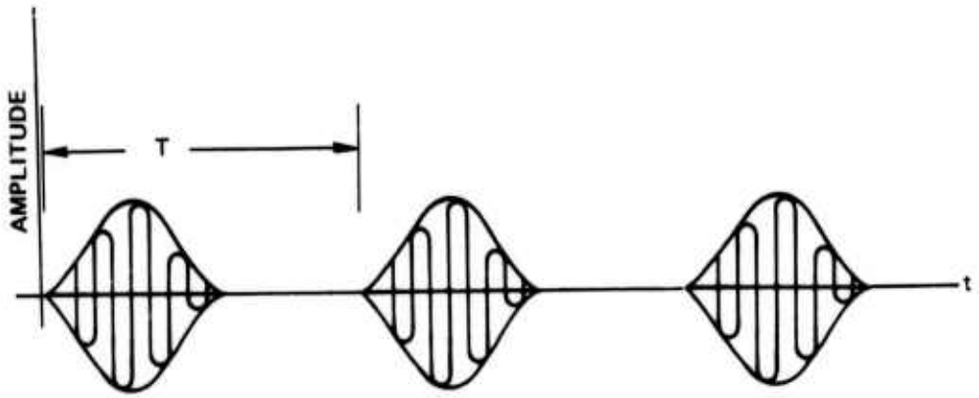

TRANSMITTED SIGNAL

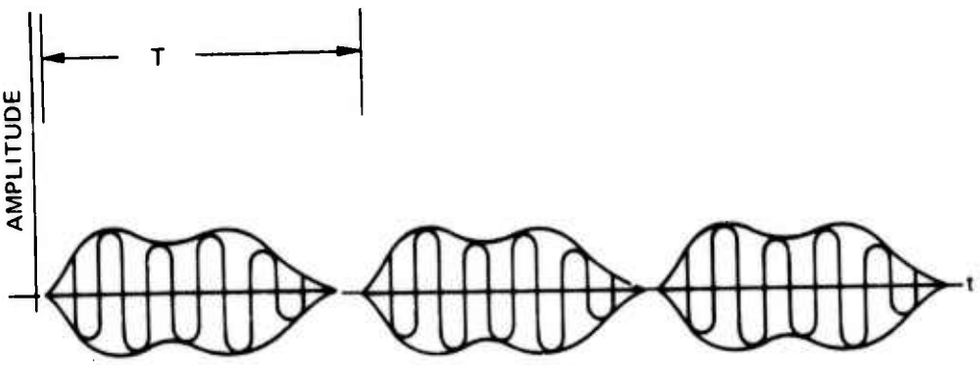

RECEIVED SIGNAL

f (t) COS ($\omega_o t + \Phi(t)$), REPEATS EVERY T

f (t) AND Φ(t) HAVE A LONG TERM TIME VARIATION DUE TO THE DOPPLER SHIFT

FIG. 3

FREQUENCY DOMAIN DESCRIPTION

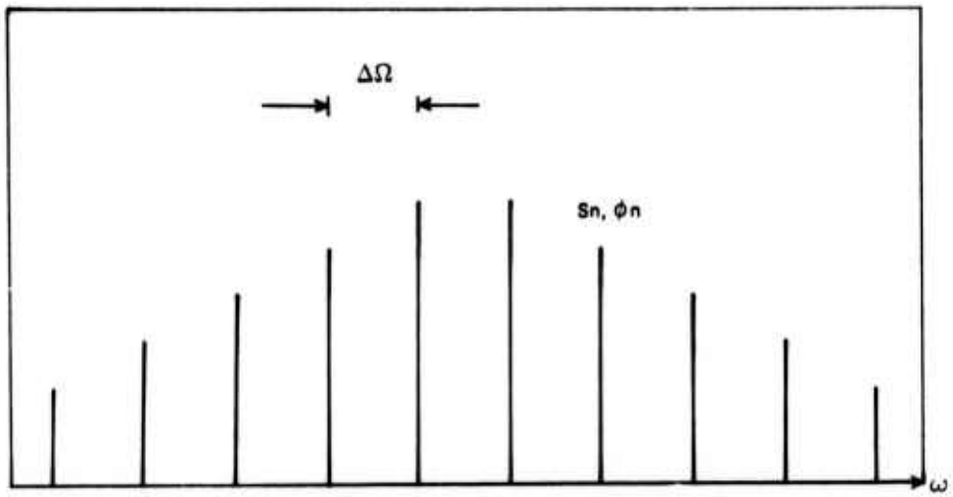

SPECTRUM OF TRANSMITTED SIGNAL

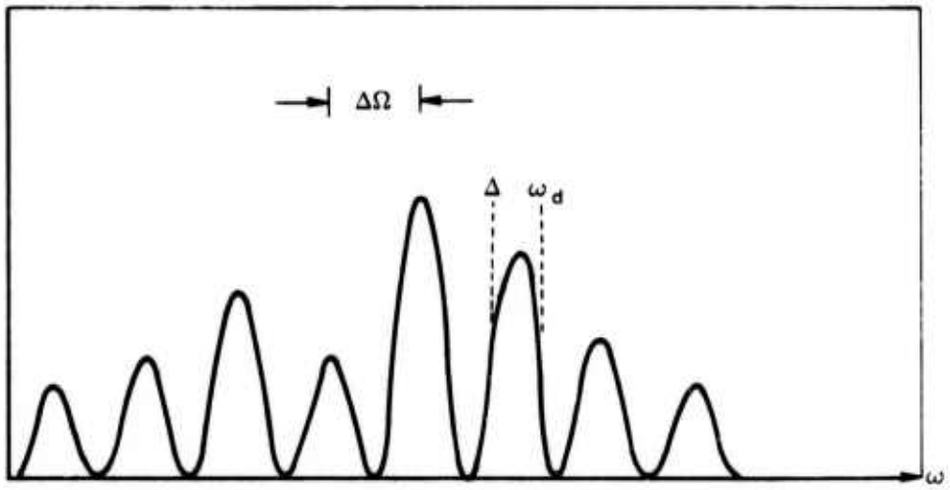

SPECTRUM OF RECEIVED SIGNAL

FIG. 4

RANGE GATING

a) ELECTRONIC

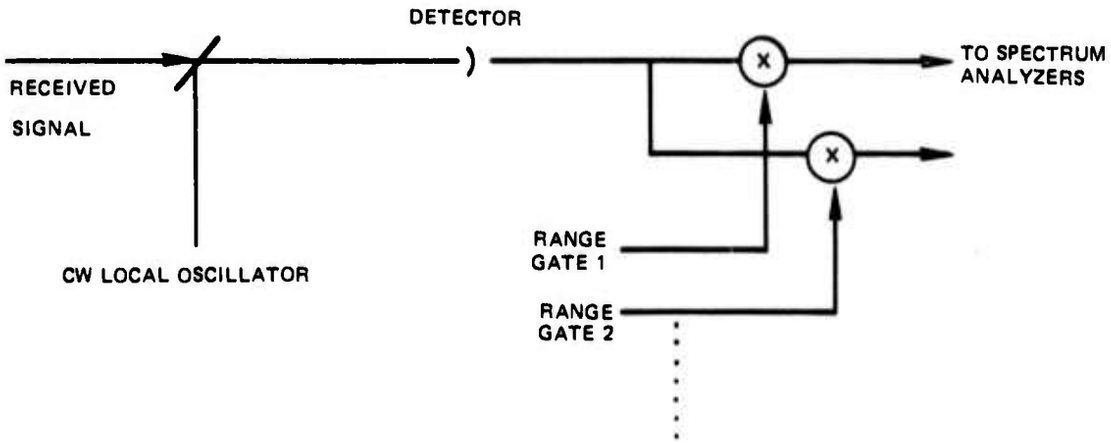

b) OPTICAL

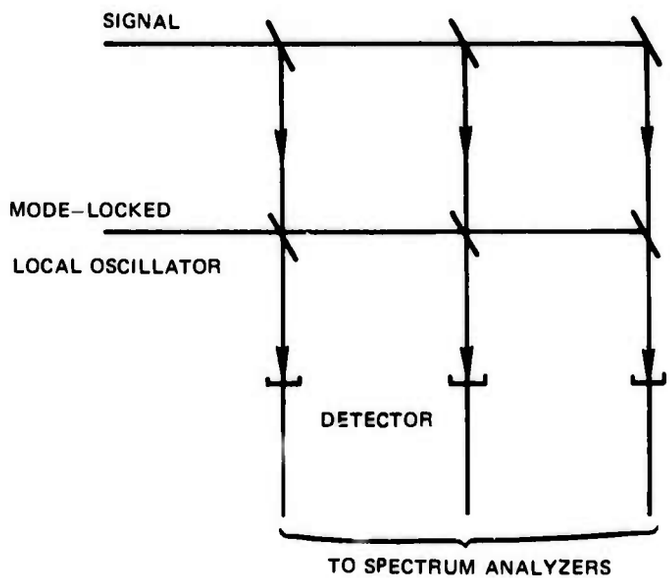

FIG. 5

EXPERIMENTAL RANGE – DOPPLER SYSTEM

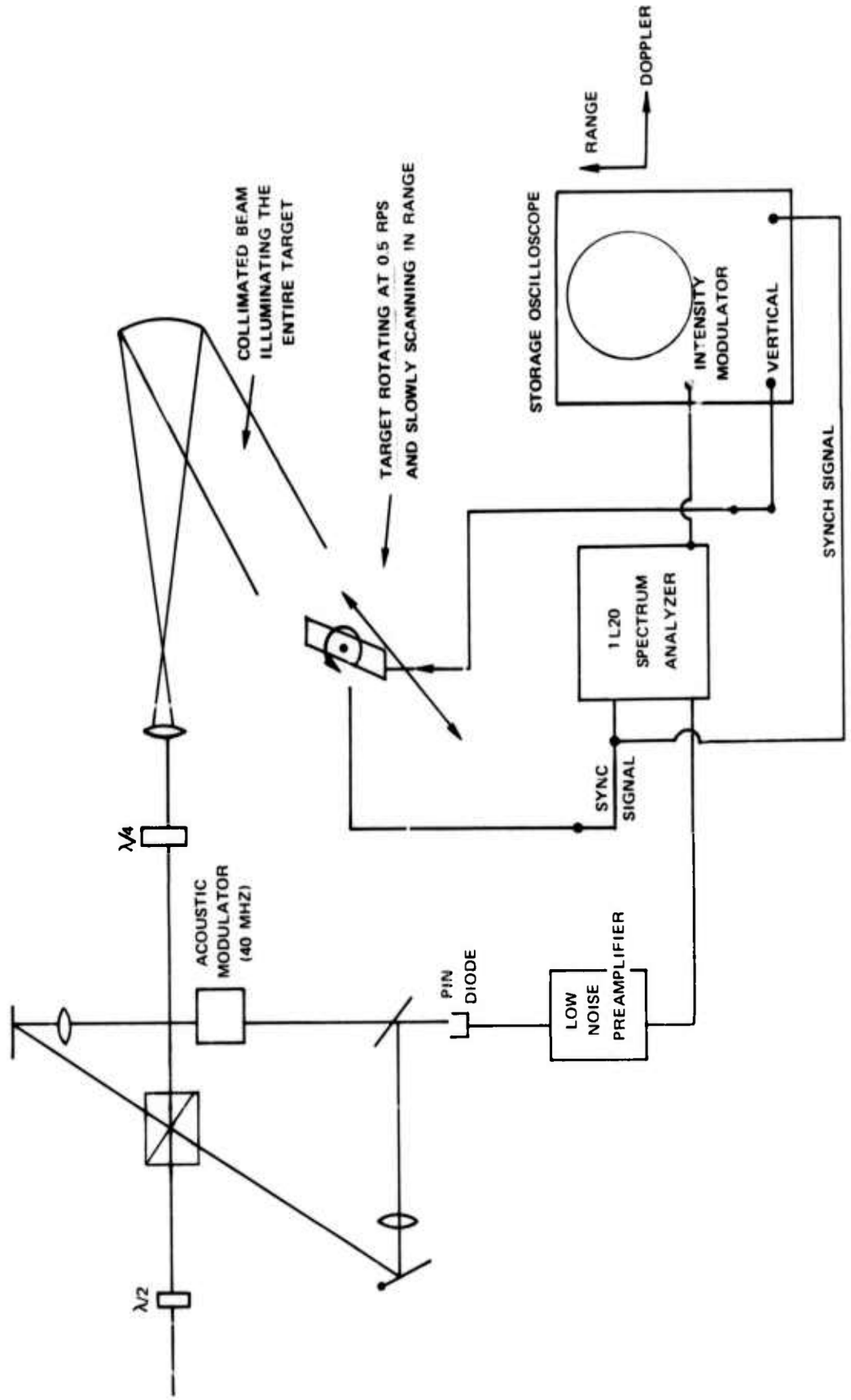

N–920479–44

FIG. 6

RANGE–DOPPLER IMAGE OF A LABORATORY TARGET

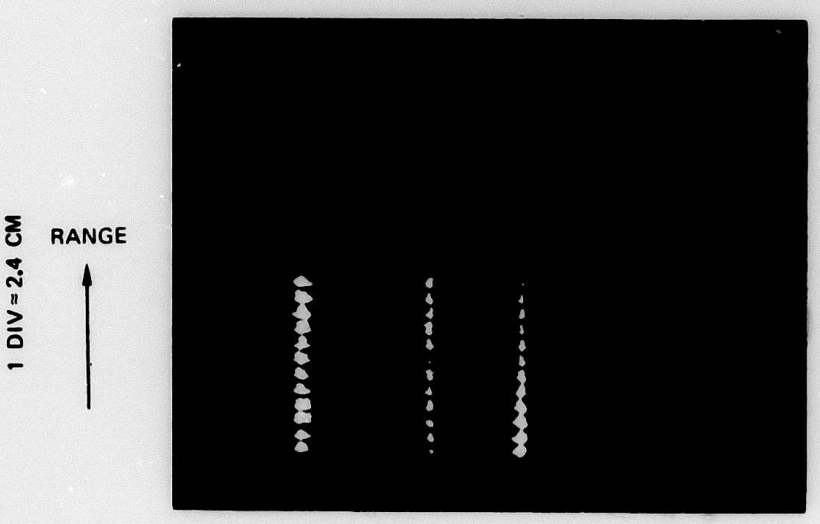

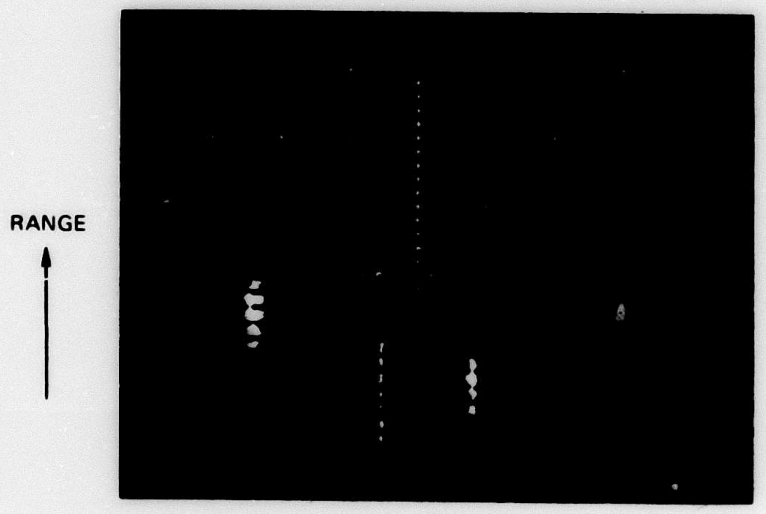

FIG. 7

GENERAL FORM OF SIGNAL PROCESSOR

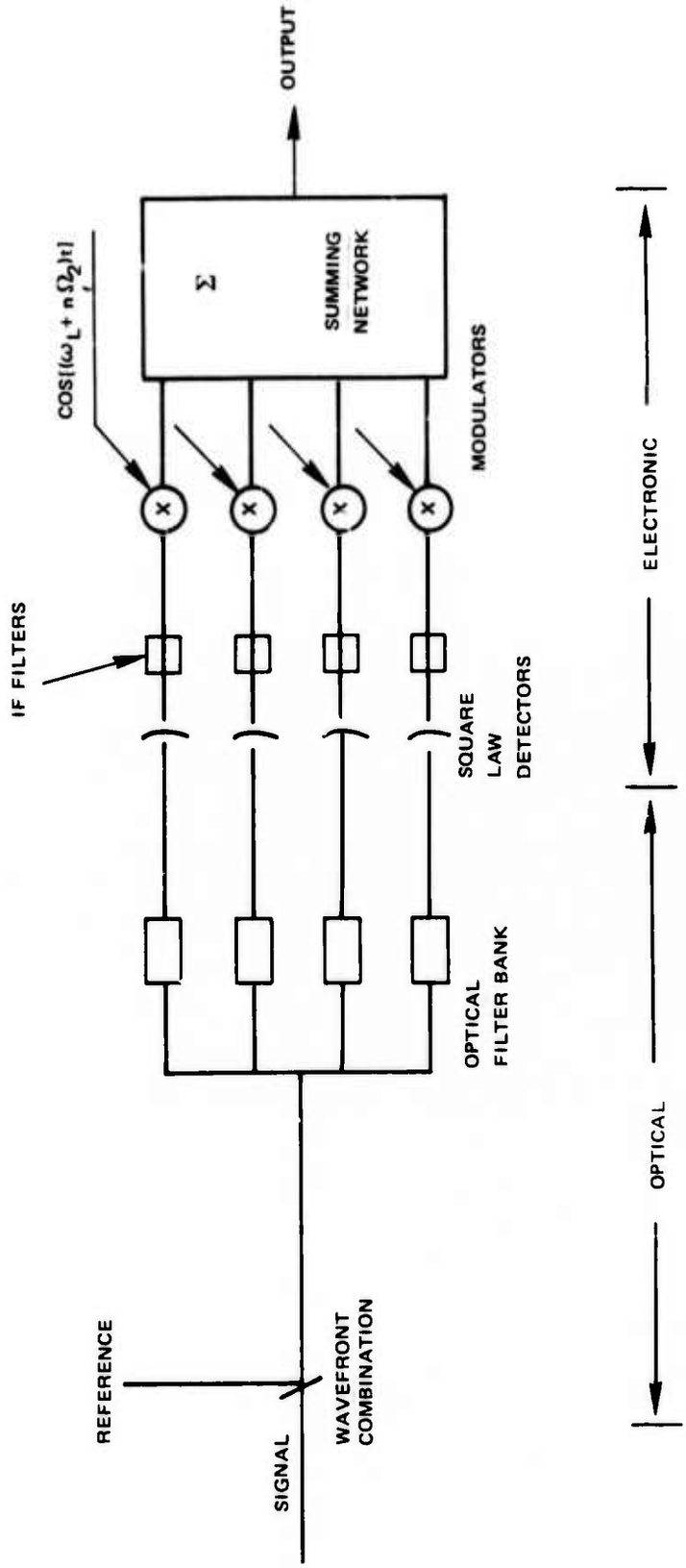

FIG. 8

SPECTRA OF SIGNAL AND REFERENCE

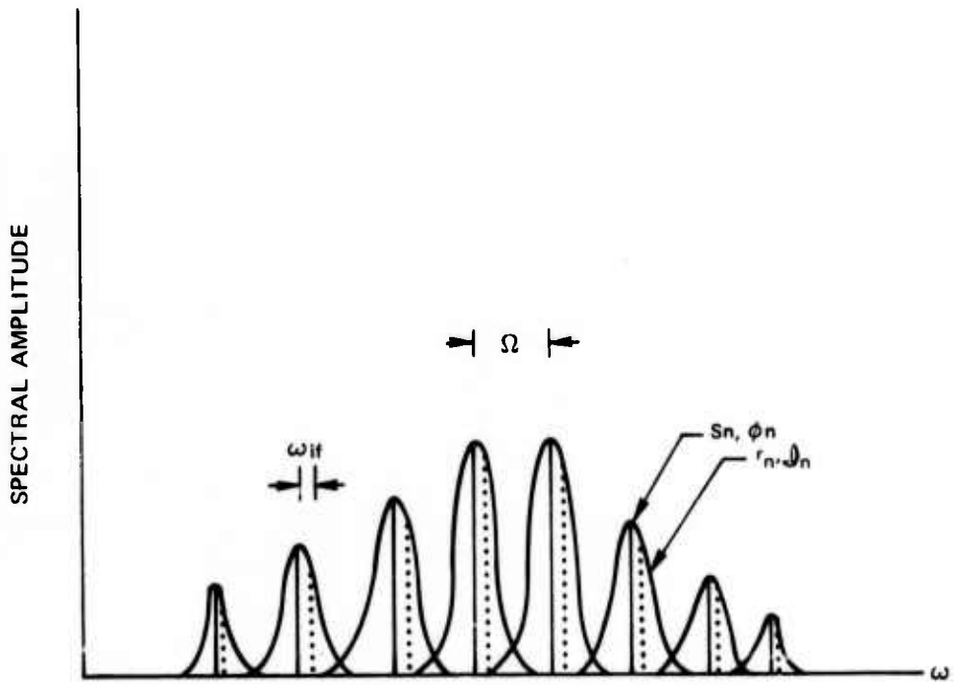

FIG. 9

FREQUENCY SAMPLING FOR A SINGLE OPTICAL TRANSIENT

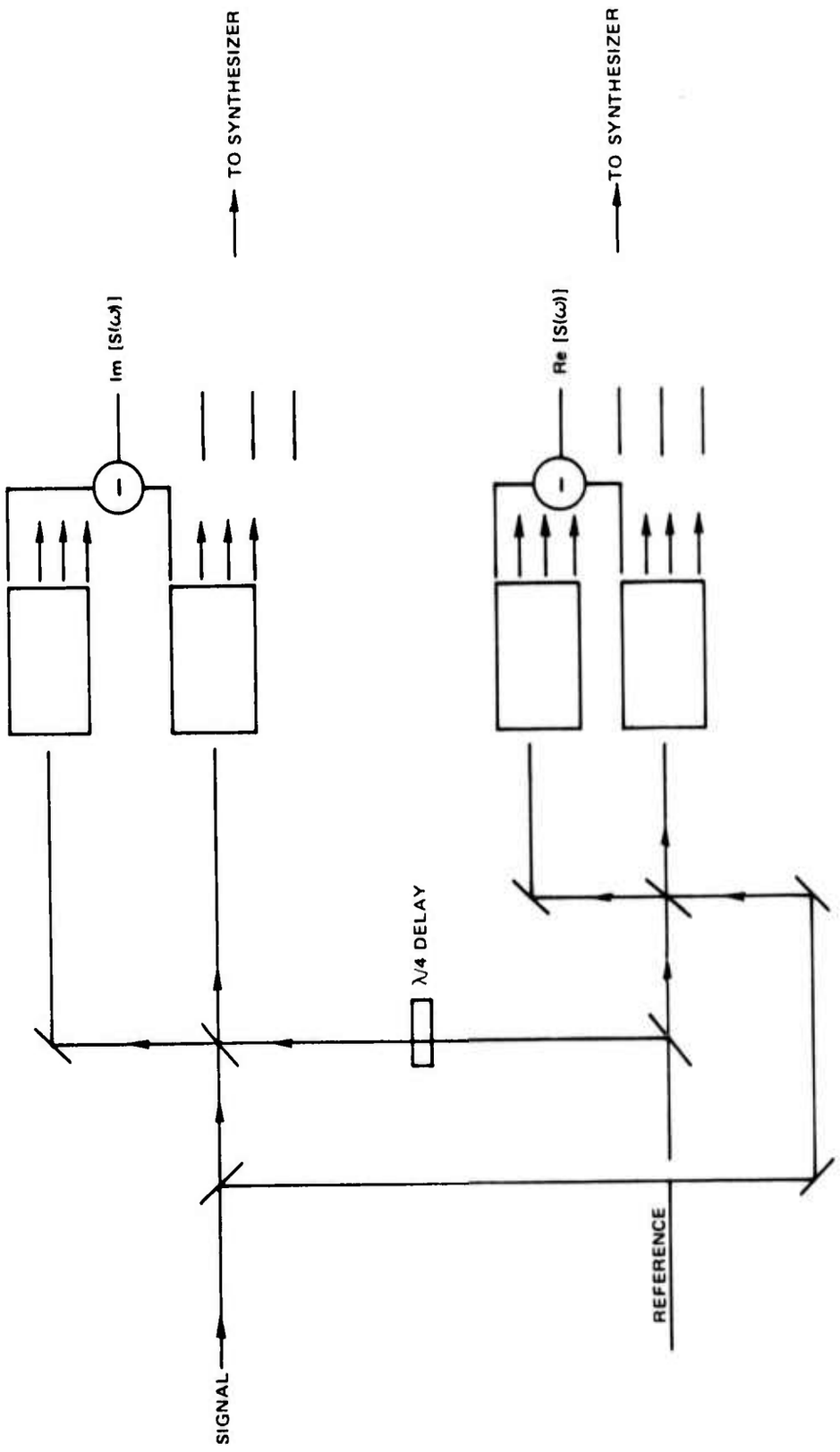

FIG. 10

BEHAVIOR OF T_c (t)

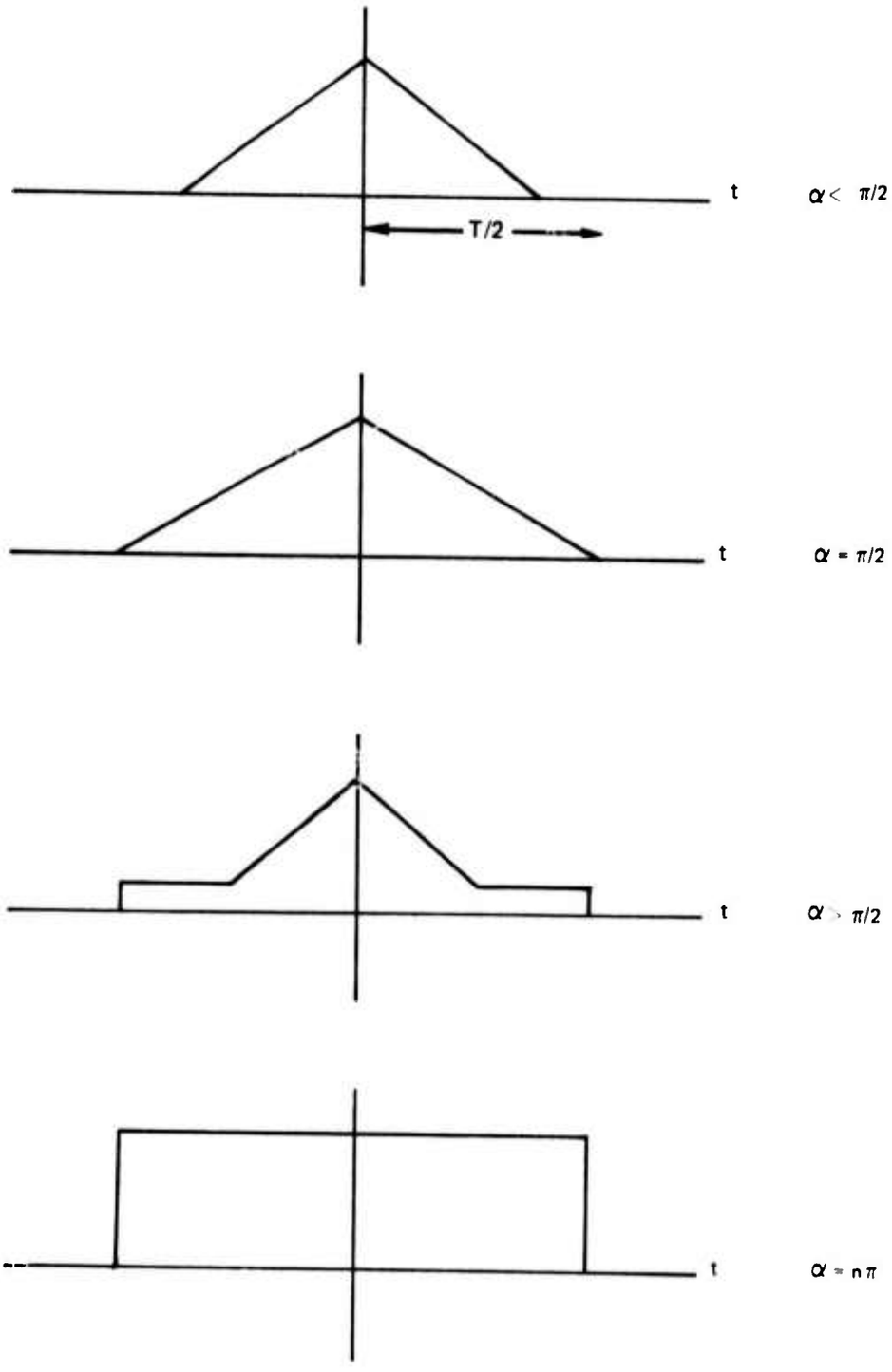

$\alpha < \pi/2$

$\alpha = \pi/2$

$\alpha > \pi/2$

$\alpha = n\pi$

FIG. 11

TRANSMISSION OF LINE SPECTRUM THROUGH FILTER

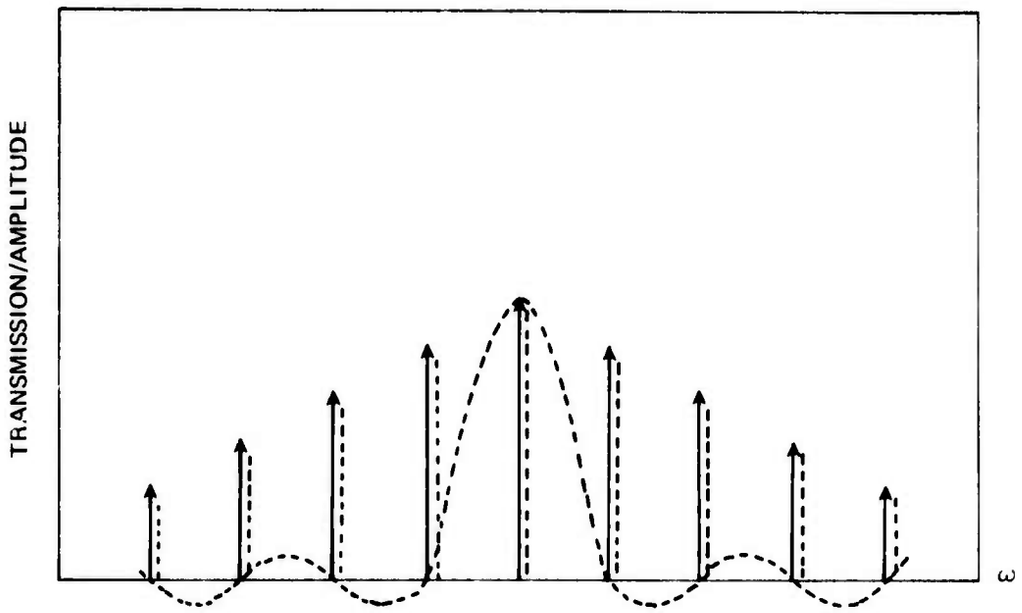

FIG. 12

RECONSTRUCTION OF AMPLITUDE STEP

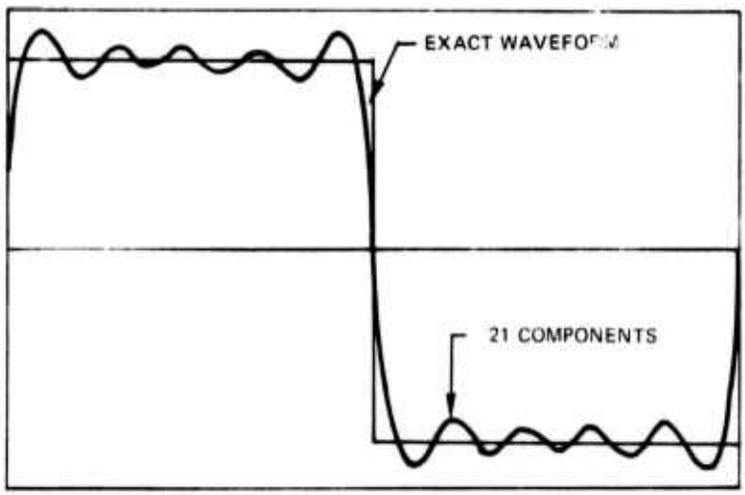

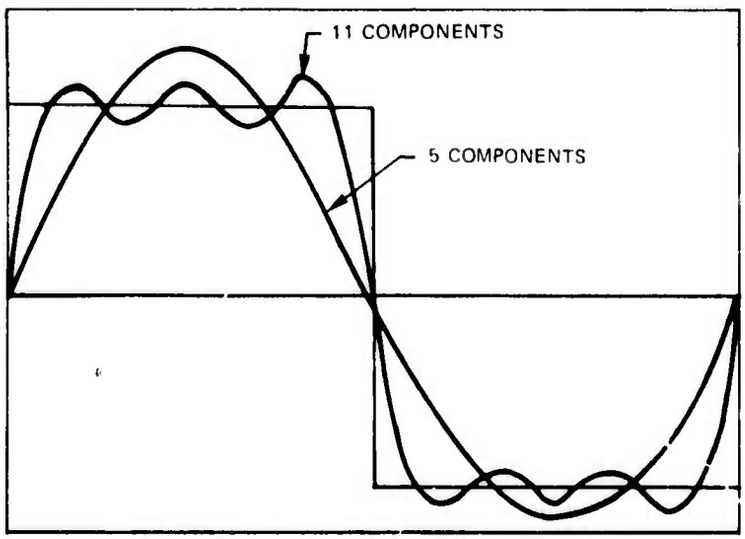

FIG. 13

RESPONSE TO FREQUENCY STEP

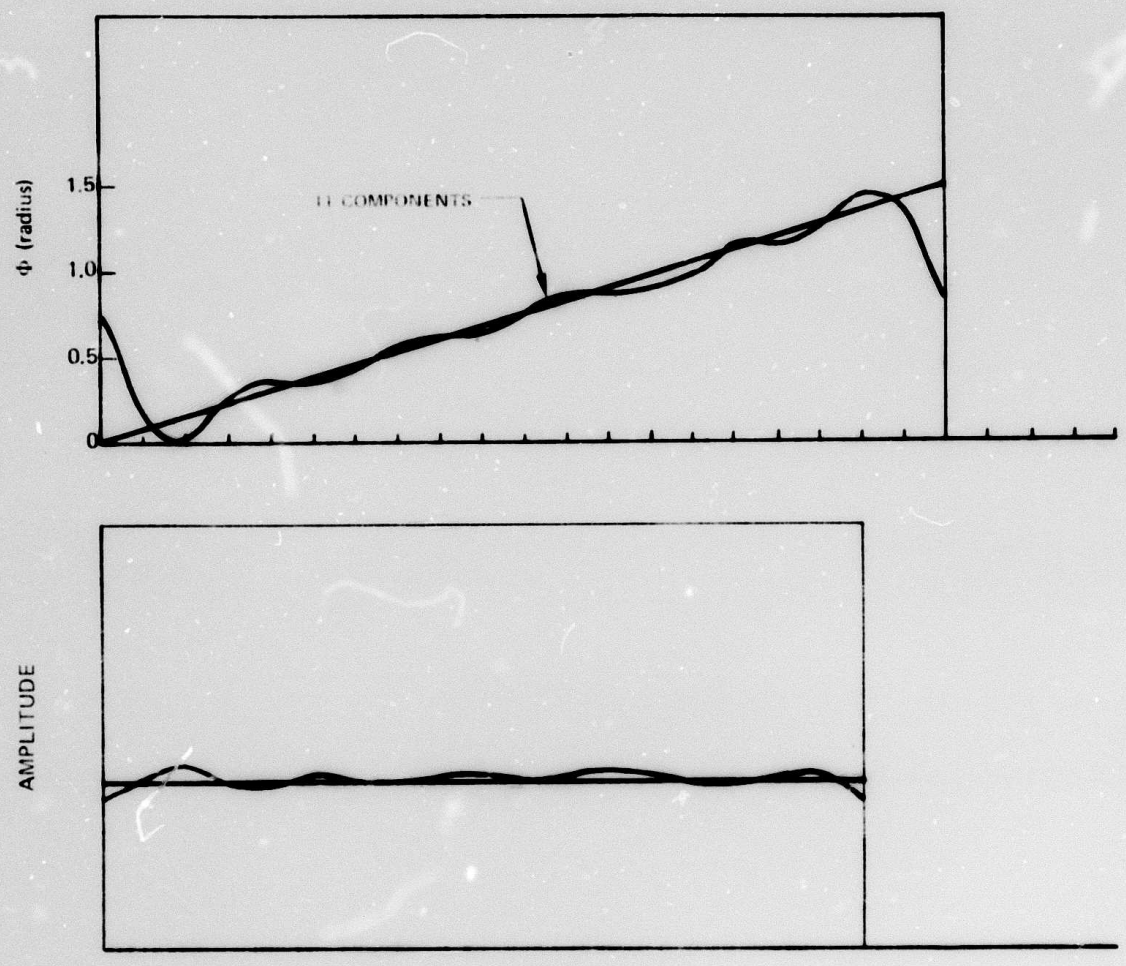

FIG. 14

RESPONSE TO FREQUENCY STEP

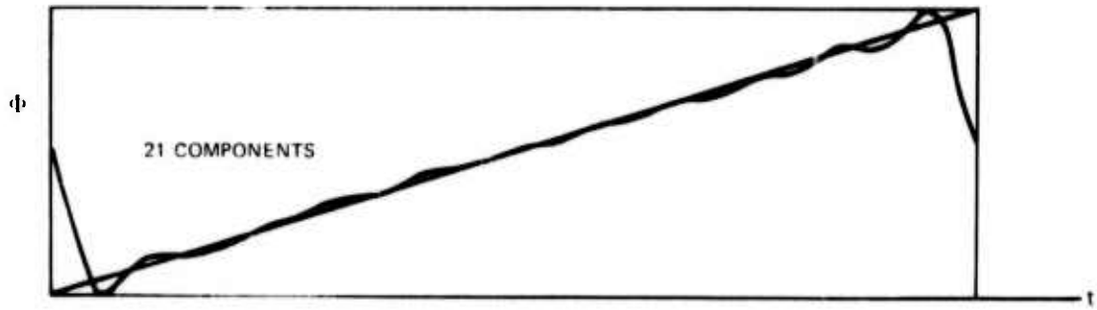

FIG. 15

RESPONSE TO CHIRPED PULSE

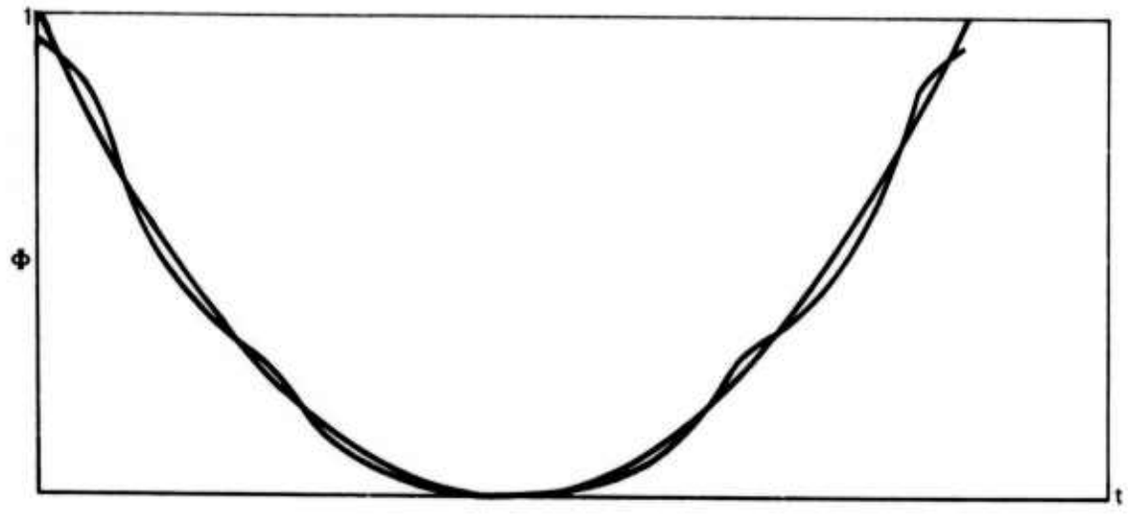

FIG. 16

RESOLUTION OF ECHELLE GRATING

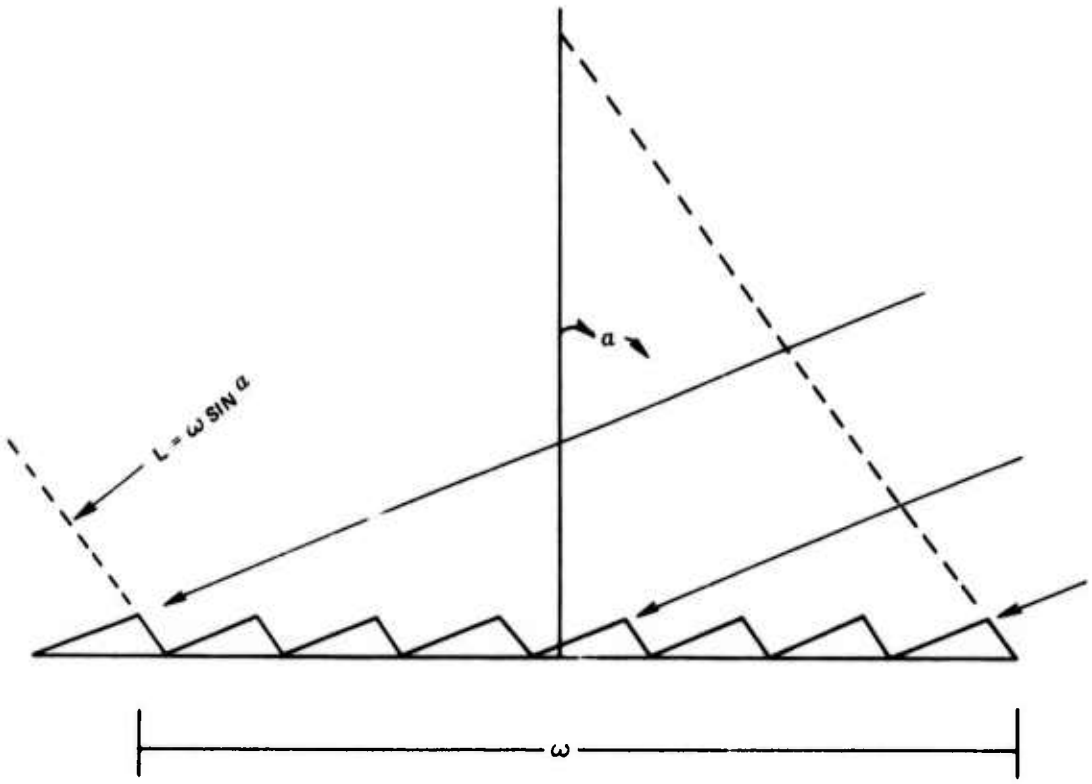

$$\Delta\tau = \frac{2L}{C} = \frac{2\omega \sin a}{C}$$

FIG. 17

ALTERNATE FORM OF SIGNAL PROCESSOR

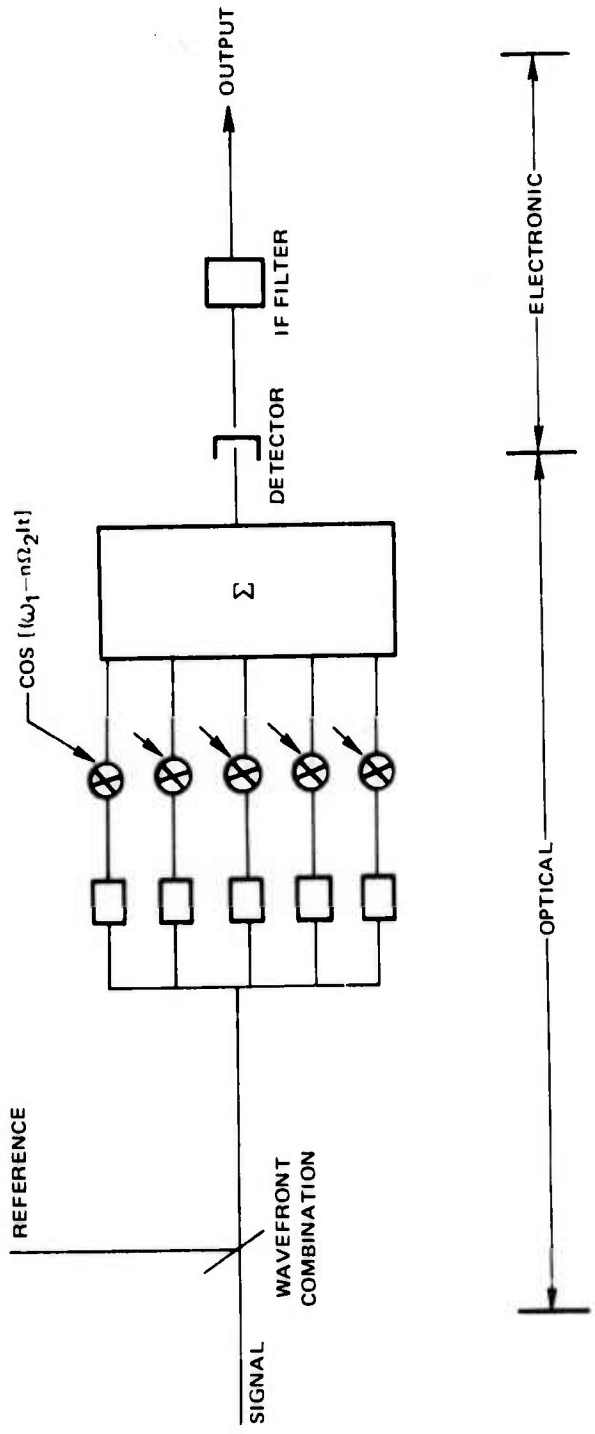

FIG. 18

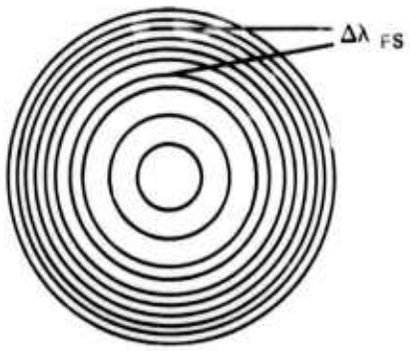

FRINGE PATTERN FROM
FABRY PEROT FILTER

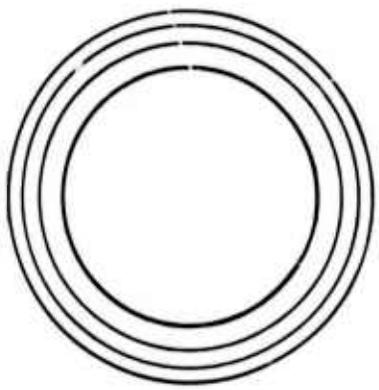

ONE FREE SPECTRAL RANGE

FIG. 19

MULTIZONE DISK

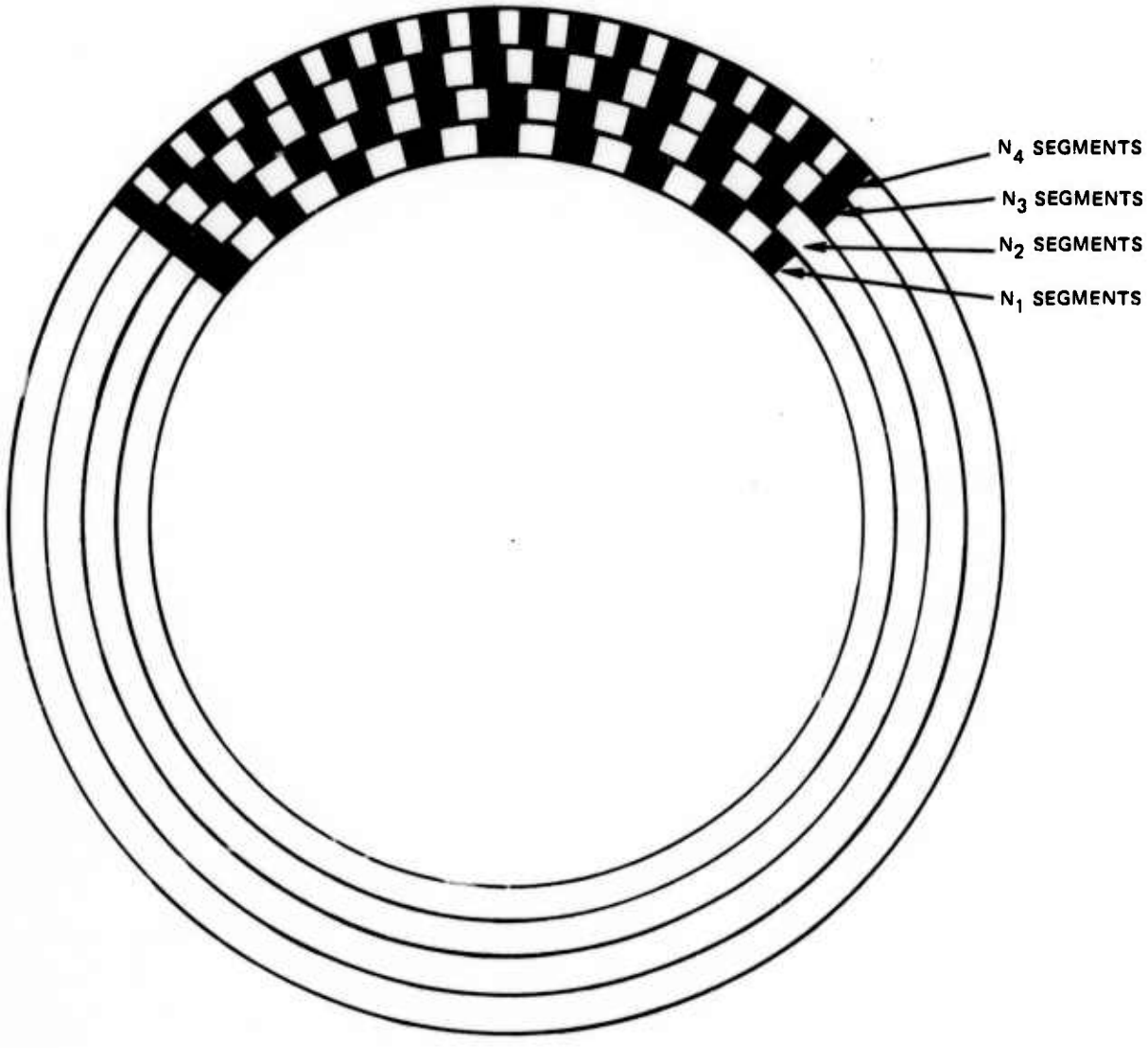

FIG. 20

MULTIPLEXED GRATING SPECTROMETER

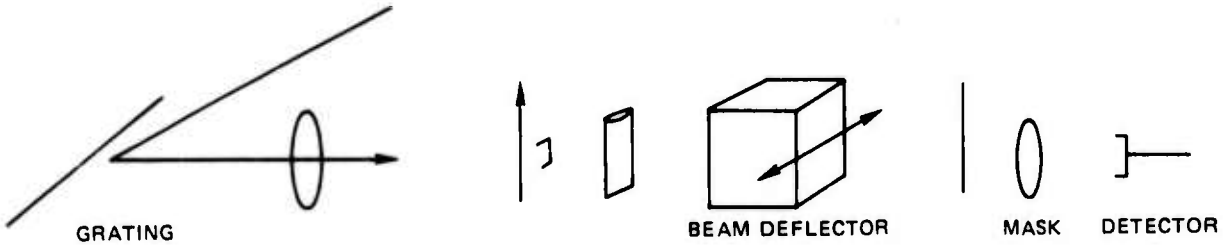

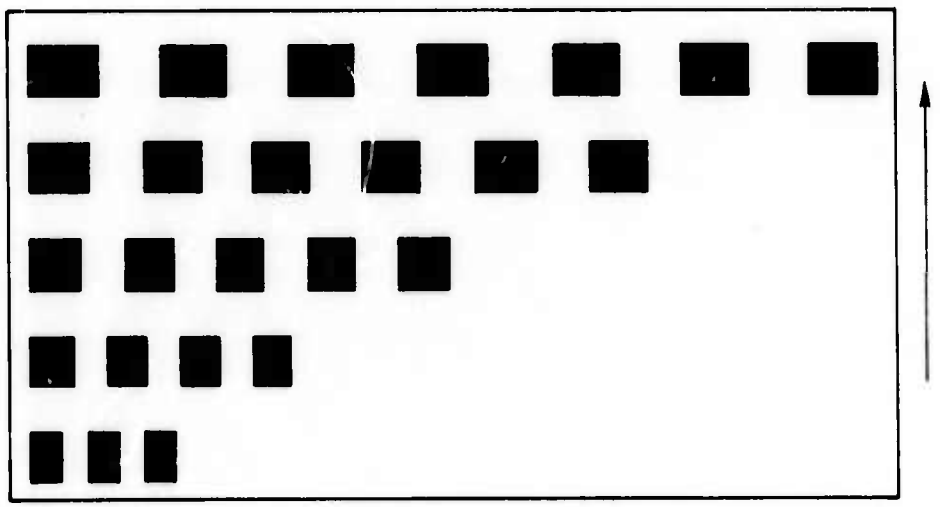

MASK (SCHEMATIC)

FIG. 21

MULTIZONE DISC MODULATOR

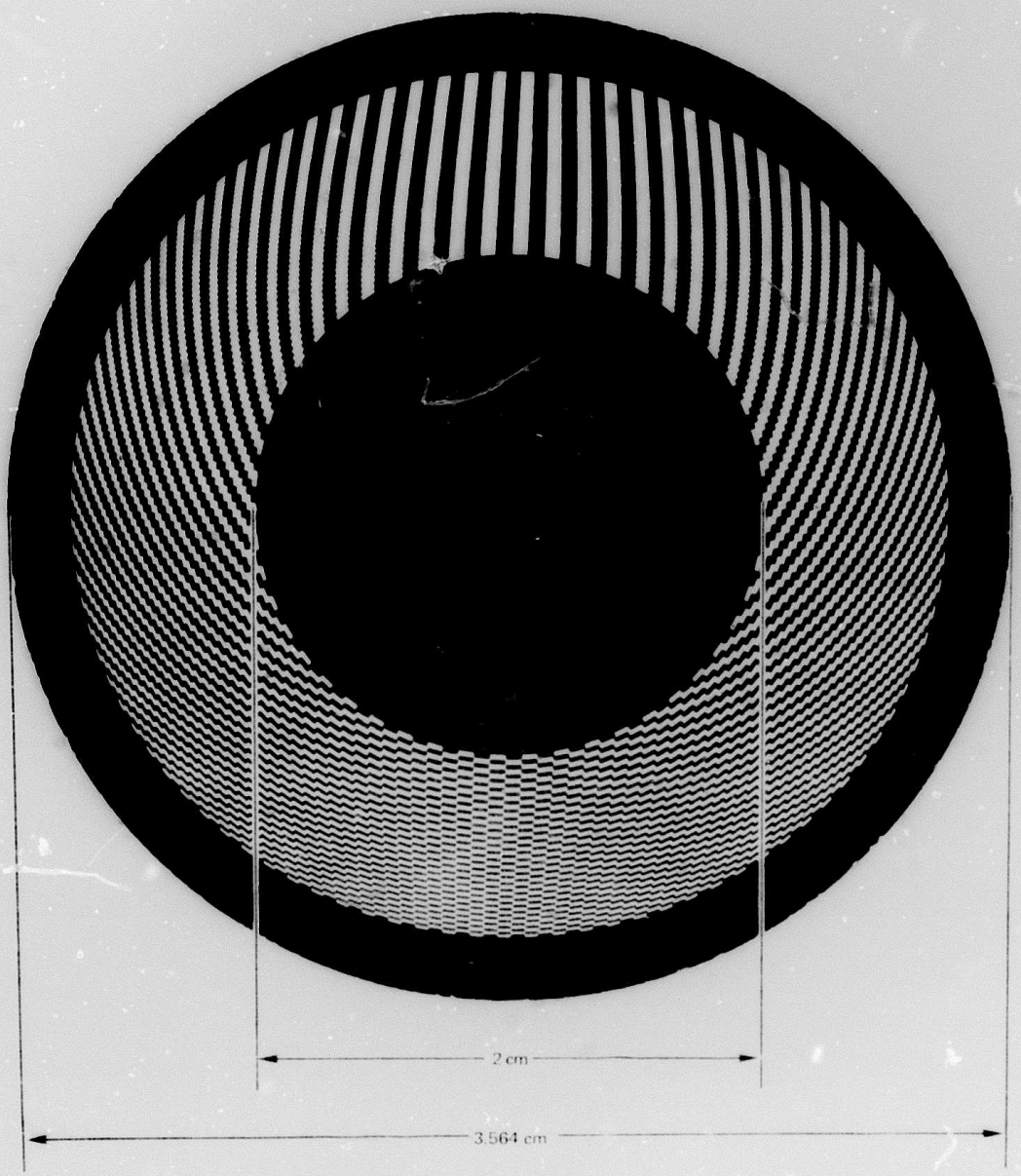

FIG. 22

FREQUENCY DOMAIN PROCESSOR (I)

OPTICAL LAYOUT

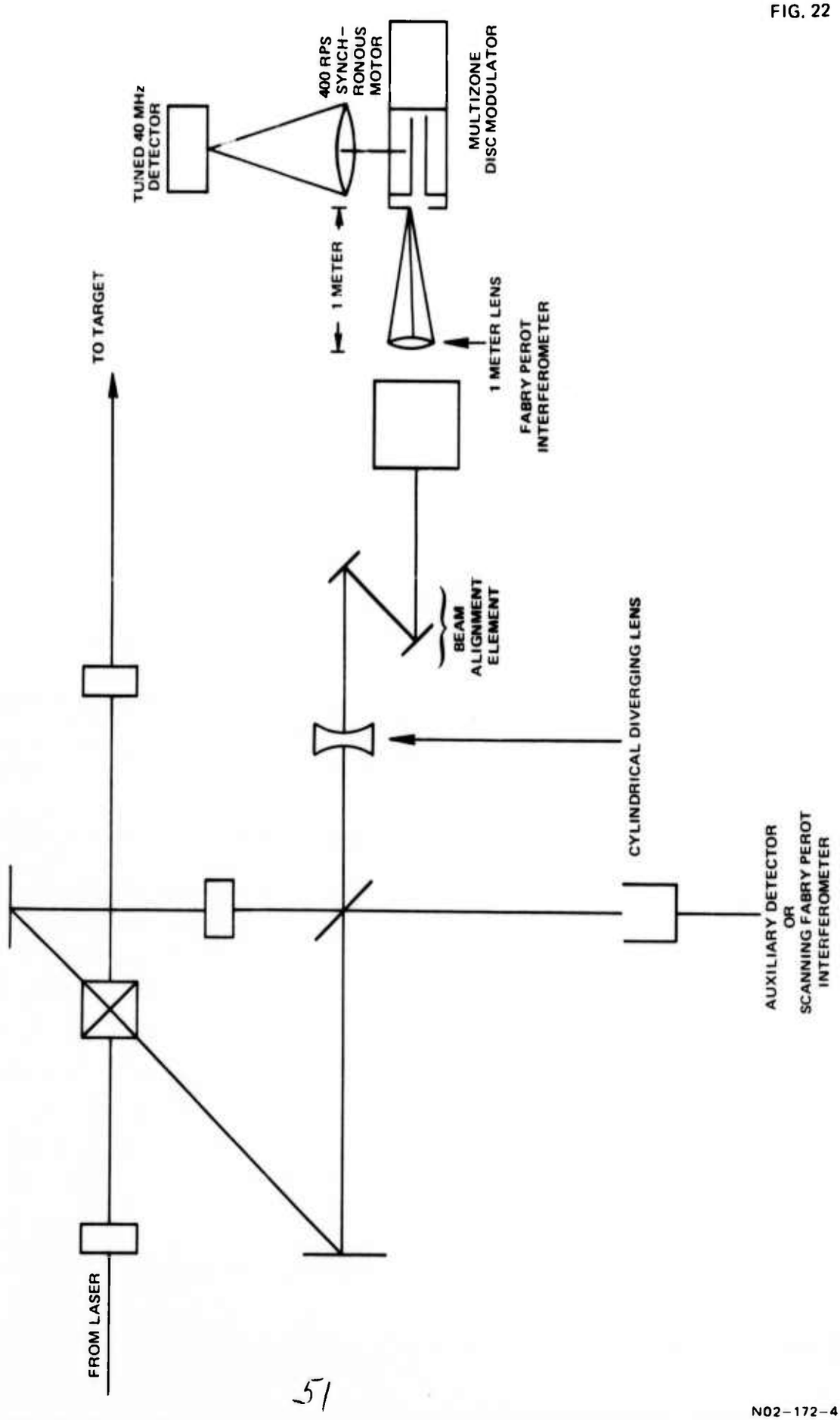

N02–172–4

FIG. 23

FREQUENCY DOMAIN PROCESSOR II ELECTRICAL CIRCUIT

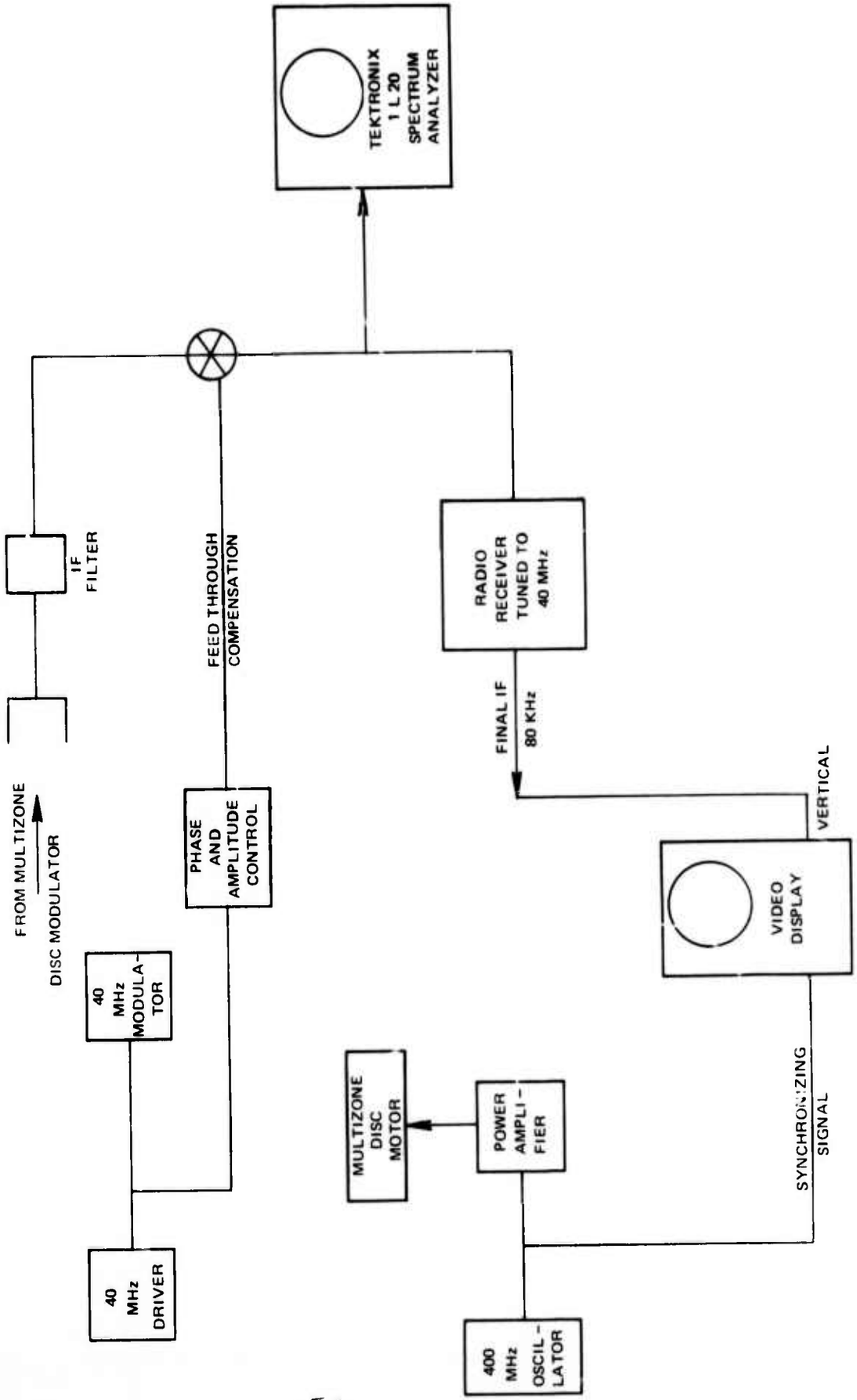

N02-172-3

FIG. 24

TRANSMITTED SPECTRUM AND RECONSTRUCTED WAVEFORM

WIDE BANDWIDTH CASE

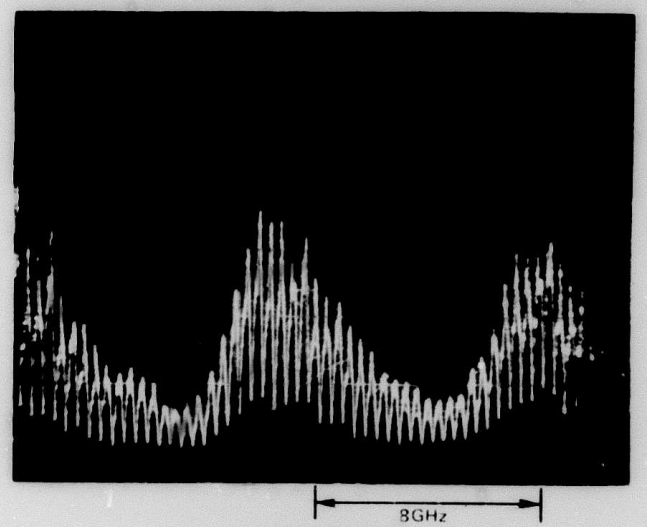

SPECTRUM

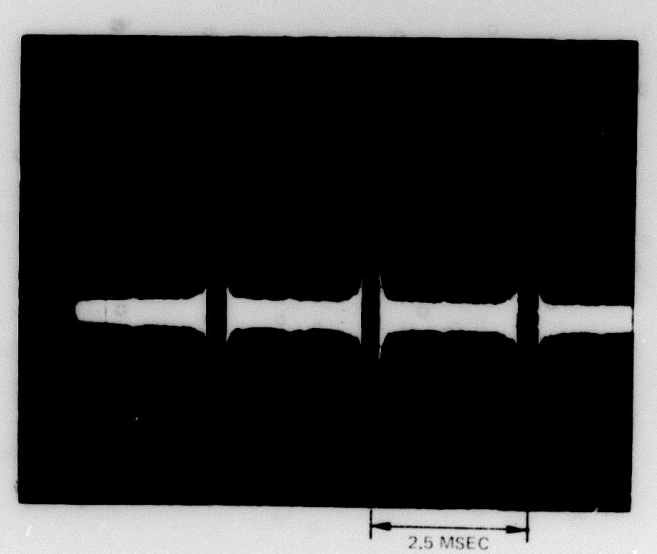

RECONSTRUCTED WAVEFORM

TRANSMITTED SPECTRUM AND RECONSTRUCTED WAVEFORM

NARROW BANDWIDTH CASE

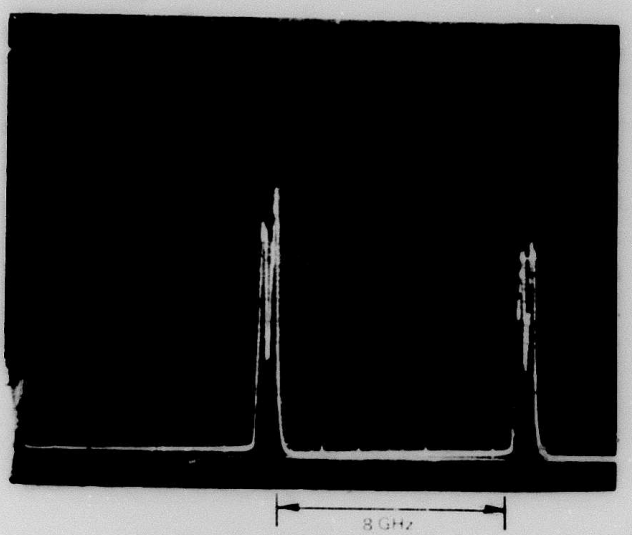

SPECTRUM

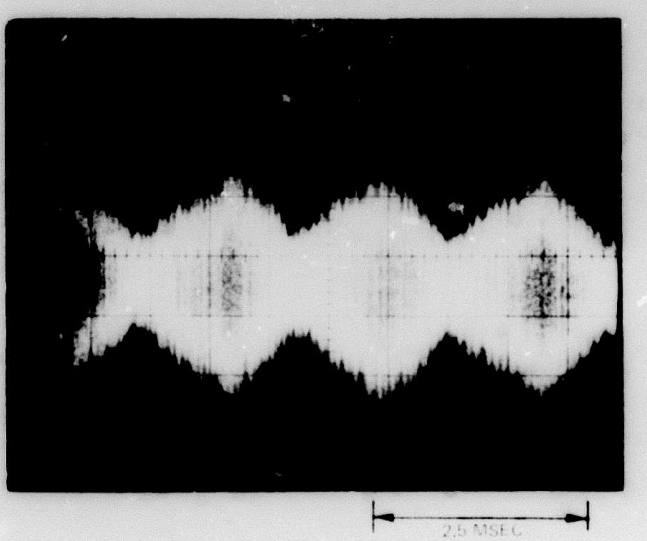

RECONSTRUCTED WAVEFORM

FIG. 26

TEST TARGET

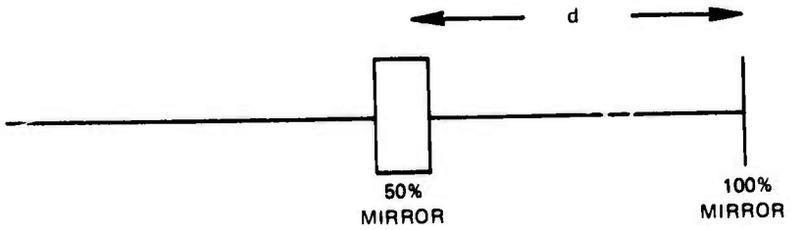

RETURN SIGNAL (SLIGHTLY MISALIGNED)

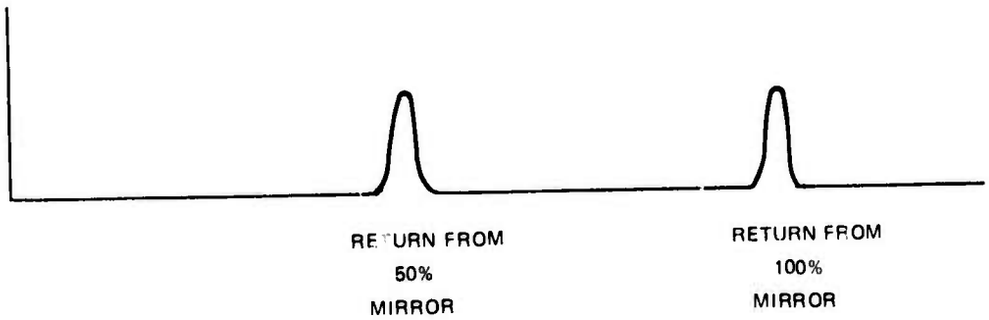

FIG. 27

SIGNAL FROM TWO MIRROR TARGET GENERATED FROM LOWER SIDEBAND

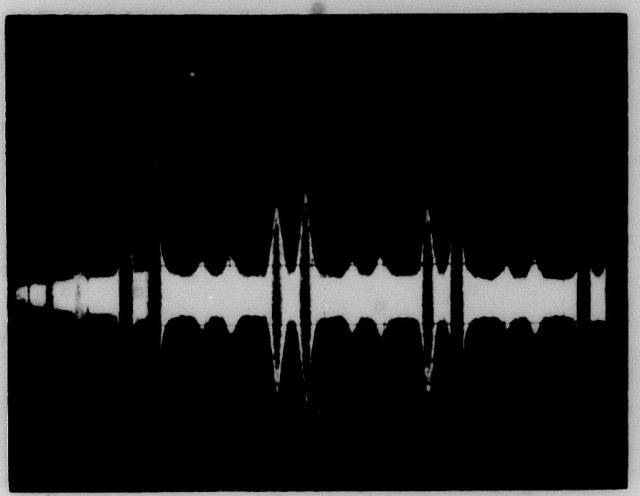

SIGNAL FROM ENTIRE TARGET

SCALE: 1 msec/cm

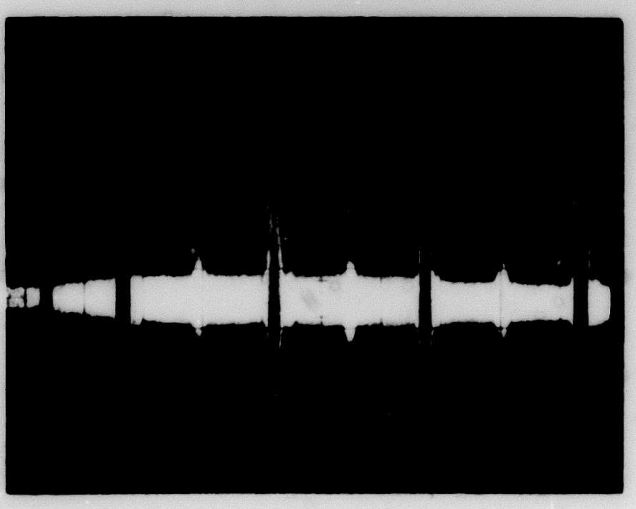

SIGNAL WITH FURTHEST MIRROR BLOCKED

FIG. 28

SIGNAL FROM TWO MIRROR TARGET GENERATED FROM UPPER SIDEBAND

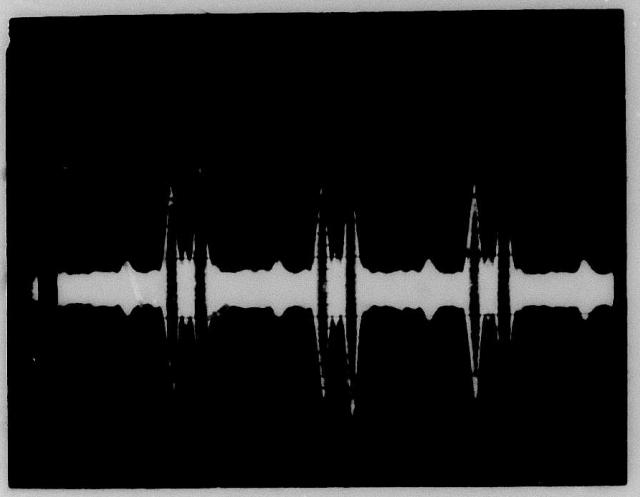

SIGNAL FROM ENTIRE TARGET

SIGNAL WITH FURTHEST MIRROR BLOCKED